A Presentation Agent for Distributed Multimedia Information Systems

by
J.A. Rody

A thesis submitted to the
School of Graduate Studies and Research
in partial fulfillment of the requirements for the degree of

M.A.Sc.
in
Electrical Engineering

Ottawa-Carleton Institute of Electrical Engineering

Department of Electrical Engineering
Faculty of Engineering
University of Ottawa
Ottawa, Ontario

1996

ISBN 0-612-15757-1

UNIVERSITÉ D'OTTAWA
UNIVERSITY OF OTTAWA

Abstract

Characterizing electromagnetic field produced by radiators in their operational modes is of primordial importance in various engineering application such as antenna design, compatibility and interference testing. The far-field pattern is the most common measure, but it is often impractical and at worst impossible to measure the far-field directly. Numerical methods implementing near- to far-field transformations rely on the knowledge of both the amplitude and phase distribution on a surface in proximity of the device under test. In certain instances however, it is expensive or very difficult to accurately measure the phase distribution component. The intent of this thesis is to investigate the feasibility of near- to far-field transformation with the premise that only amplitude distribution component is available. The requirement is thus to provide, or estimate, the missing information necessary for near- to far-field transformation. The retained approach implements the well known spherical wave expansion technique. The coefficients of the spherical wave functions depend on the boundary conditions, and due to their incomplete knowledge only bounds for those coefficients can be calculated. Application of heuristic methods to the estimation of the coefficients, and upon the assumption of the uniqueness of the solution, are sufficient to predict the radiated fields. This method presents an important advantage over direct phase distribution estimation in that the number of coefficients is well defined and can generally be expected to be less than the required number of phase measurements.

Acknowledgments

I wish to thank Dr. G. Costache and Dr. E. Petriu who made this research possible. I also extend my heartfelt gratitude to people too numerous to mention herein for their constant support.

Contents

List of Figures

List of Tables

Chapter 1

Introduction

1.1 Motivation

The possibility of determining the far-field pattern of radiating systems by measuring its corresponding near-field presents numerous advantages over the direct measurement of the far-field. For accurate direct far-field measurements a calibrated open site test range is required: in some instances though, the distance to the radiating far-field might be greater than the open site itself, or the reflections from nearby objects could introduce an intolerable amount of error. In certain circumstances, moving the device under test to and from an open site test range adds to the inconvenience. Due to these, and other problems, alternative methods such as near- to far-field transformations have been developed.

However, various difficulties inherent to the near-field measurement and its subsequent transformation to the far-field have to be overcome before they can be successfully applied to EMI/EMC and antenna characterization problems. Amongst the most important limitations of those methods are,

I. necessity for precise phase measurements of the sampled near-field points which are critical in correct far-field prediction,

II. the size of the problem domain can be overwhelming in computer power requirements, making the task all but unrealizable from a practical point of view.

The purpose of this dissertation is to present a phaseless near- to far-field transformation technique, thus addressing point I above, coupled with practical

considerations for minimization of computing time as outlined in point II. rendering the proposed approach more than just of academic interest.

1.2 Contribution

This dissertation addresses points I and II outlined in the previous section. Most of the research in literature deals with simplified cases where the knowledge of the phase distribution is implicitly assumed. An extensive literature survey is included in Chapter two, and serves as a starting point for finding an appropriate method of phaseless near- to far-field transformation. Relatively few of the presented methods deal explicitly with amplitude field measurements only, and those that do consider simplified one or two dimensional geometry. The proposed approach considers a general three dimensional case without any assumptions as to the probable radiation pattern, making it suitable for electromagnetic interference and compatibility measurements.

Regarding the first point, acceptable phase measurements can be performed up to a certain frequency range, depending on the measuring devices used. At higher operating frequencies or due to measuring equipment with limited precision, the phase measurement will introduce a discouraging amount of error in subsequent calculations. This problem can be circumvented by performing amplitude measurements on at least two surfaces enclosing the radiator. The amplitude samples can be obtained with a relatively high degree of accuracy at any frequency, enabling the implementation of a phase retrieval procedure. The knowledge of both the amplitude and phase on a surface enclosing all inhomogeneities is both sufficient and necessary to completely characterize a general radiated field.

The near- to far-field transformation is a numerical procedure, and as such an approximation is made of the continuous functions involved. The radiated near-field is first approximated by field samples. The amount of samples necessary to achieve an acceptable level of accuracy will depend on the chosen method of transformation. As a rule of thumb, the more samples we gather, the more accurate results we obtain after the

applied transformation. Obviously, the result's accuracy has to be weighted against the associated computing time requirements, and a proper optimum number of such samples found. Similarly, the usage of such methods yields the electromagnetic fields at discreet locations only. Whether the samples are sufficient to represent the far-field in a given radiation plane is obviously of importance if we are interested in more than just rough knowledge of the far-field radiation pattern. Again, a trade-off analysis of the number of samples against computing requirements is in order. In EMI/EMC applications, no assumptions about the radiator are made so that a fixed number of samples may very well prove either insufficient or redundant in the resulting calculations. However, a minimal number of samples for a general problem domain, dependent only on the size of the radiating system and the frequency of operation, can be derived from the analysis of the radiated fields. This set of optimum number of samples can then be used to reconstruct the electromagnetic field with standard digital signal processing techniques, cutting down dramatically on the computing time and power requirements.

1.3 Organization

The present dissertation is composed of six chapters. In the second chapter a literature review is presented on all relevant topics covered herein. Chapter three covers the theoretical background, and chapter four presents the proposed approach. Chapter five presents the results of the performed simulation. Finally, chapter six presents the conclusions and outlines future research possibilities.

Chapter 2

Background Information

2.1 Near- to Far-Field Transformations

Both the electromagnetic interference and compatibility compliance tests and the characterization of the antenna radiation patterns require the knowledge of the radiation in the far-field of the device under test. In both cases it is often impractical or impossible to provide an open range suitable for direct far-field measurements. An elegant way to bypass this problem is to collect measurements in the near-field of the device, usually in a controlled environment as provided by an anechoic chamber, and to calculate the far-field by way of mathematical transformations.

There are other methods of far-field determination beside the mathematical transformations of the field and they will be mentioned here for completeness sake. A much more complete analysis of these methods is presented in [17] along with guidelines of the procedures to follow. By creating a plane wave in close proximity to the antenna under test simulating an irradiation by a source placed in the far-field, the far-field characterization can be obtained by reciprocity principle. Applicable to certain types of antennas only, the second method focuses the radiation in the near-field, and the resulting measurements are assumed correct with an obvious error tolerance.

Two fundamentally different approaches have been applied to determine the far-field radiation from the knowledge of the near-field radiation of a radiator using mathematical transformation methods. The first is based on the principle that the complete electromagnetic field configuration surrounding a radiator can be computed if either the current or charge distribution over radiating structure is known exactly. In this approach, measurements of the electric or magnetic field in the direct vicinity of the system are necessary [25].

The second approach is based on expressing the total electromagnetic field in terms of a modal expansion. The amplitudes and phases of these modes can be derived from the knowledge of the electromagnetic field over an appropriate surface, planar, spherical or cylindrical. The exact distance of the measurement points on such a surface from the radiator itself is not critical and permits to express the radiated field outside such a surface, including the far-field region.

As examples to the described techniques, the following papers present their approach and results; in [23] the field is expanded into a cylindrical series expansion and the coefficients are calculated via a Fourrier transformation of the measured near-field. The results restricted to the two dimensional space, compared successfully to the predicted results, and a discussion is presented on possible extension of the method to the three dimensional geometry; additional results are presented in [40]. In [26] an algorithm is developed based on the finite-difference time-domain (FDTD) method. For validation, far-field results for a flat plate are transformed to the frequency domain and compared with results obtained with the method of moments. In [27] a sampling algorithm based on plane-polar measurements properties is formulated. Optimal sampling densities and measurement surfaces in terms of shapes and positions was analyzed in order to simplify and improve the transformation. The plane-rectangular near-field samples are accurately recovered from the plane-polar ones, enabling the standard FFT to be applied. Authors report an important reduction in both in measurement time and memory storage requirements. A technique presented in [21] uses the concept of equivalent currents to replace the radiating system. Data from planar, cylindrical and spherical near-field measurements can be used, and for practical problems conjugate gradient method has to be applied in order to solve the large system of linear equations. Methods for near- to far-field calculations of two-dimensional combined finite element and absorbing boundary are presented in [22]; three methods are described in terms of accuracy, efficiency and capabilities: harmonic expansion (cylindrical waves) Green theorem integral and volume sources integration. For plane apertures and flat reflectors, [30] uses a formulation whereby the surface double integral is transformed into a line integral around the boundary. Further, if this boundary is a polygon, the line integral can be reduced to a

closed form expression eliminating the need for integral expressions. The usage of such line integrals reduces sharply the computer calculations requirements. The far-field and the radar cross section are evaluated by transformation of the results of the transmission line matrix (TLM) method in [31]. Two methods are proposed, one based on equivalence principle and the second on the Kirchhoff theory of integration in order to reduce the complications associated with numerical methods based on differential equations. In [32] spherical wave vectors are used to find the far-field at observation points are restricted to a single ϕ-plane at a time. The analytical expressions are much simplified and the method provides very good accuracy but at the expense of computational time. The proposed exact analytical technique can be applied to probe-directivity uncompensated spherical near- to far-field transformations for large radiators. The method presented in [41] makes use of pseudo-sampling to predict the far-field radiation. In the case of the Fresnel small angle approximation, the far-field reconstruction based on near-field samples will not require matrix inversions, improving the methods overall efficiency. The criteria to be satisfied in order to obtain a valid Fresnel approximation are presented in [45].

Most of the authors consider both the absolute and relative error level impact on the overall accuracy and stability. For a general case, the error of the recovered far-field due to random noise, is analyzed in [33] where the error is treated as added random variable whose distribution is to be found. Results are presented for cylindrical geometry, and can be used as part of complete near-field error analysis.

Although an integral part of any attempt for practical implementation, the proper selection of a probe measuring the scattered electromagnetic field is left out of this dissertation. For an overview on electromagnetic probes [43] and [44] should be consulted. Mutual coupling between the device under test and the probe, which affect the measurement values are described in [35]. The assumption that the measurement of electromagnetic field is readily available will simplify enormously the presented concept. If this were not the case, factors such as the probe intrusiveness (field transparency), directivity, frequency response, sensitivity and ability to measure the field at essentially one point in space would have to be considered.

2.2 Near- to Far-Field Phaseless Transformation Methods

Phaseless measurements find application in characterization of antennas at millimeter and sub-millimeters wave bands where accurate phase sampling becomes increasingly difficult.

Two problems arise when dealing with the problem of recovering the far-field radiation from amplitude only measurements. The first deals with the *uniqueness* and the *stability* of the obtained result. The second arise since the actual determination of the solution necessitates an iterative algorithm which searches for the solution by minimizing a convex objective function. The speed of the convergence of the algorithm could be too slow for practical implementations, or the solution could arrive at a local minimum and remain trapped within, yielding an inaccurate solution.

In [28], a phaseless cylindrical near- to far-field transformation algorithm is described. The method implemented is presented in Figure 1.

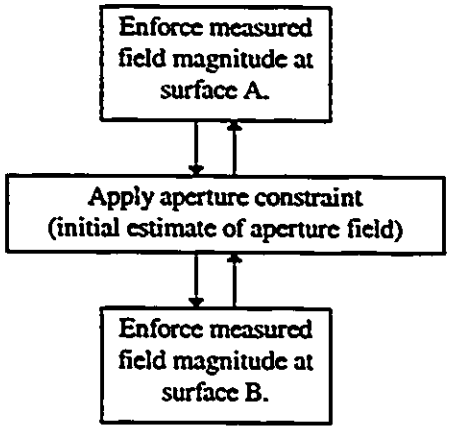

Figure 1 Phase retrieval algorithm

In this implementation, sample intensity data points are measured on two cylindrical surfaces surrounding the antenna. The knowledge of the antenna geometry simplifies the resulting calculations. Two sets of measurements are made at separate distances on cylindrical surfaces. An initial guess at the complex aperture field distribution is made, possibly including all *a priori* knowledge about the antenna and

field distribution. In the case when no such extra information is present, uniform distribution is assigned as the starting guess. The aperture field is then transformed to one of the measurement surfaces where the intensity data are enforced. The new distribution is subsequently transformed to the aperture plane. The same procedure is applied to the second surface, and the process is repeated until satisfactory convergence has been attained. The field transformations applied in the algorithm are derived from the cylindrical wave equations,

$$E_z(r,\phi) = \sum_{n=-N}^{n=N} a_n H_n^{(2)}(\beta r) e^{-jn\phi} \tag{2.1}$$

noticing that this can be expressed as,

$$\mathcal{F}\left[E_z(r,\phi)\right] = a_n H_n^{(2)}(\beta r) \tag{2.2}$$

where $\mathcal{F}$ denotes the Fourrier transform. The field distributions are related by,

$$E_z(r_b,\phi) = \mathcal{F}^{-1}\left\{\mathcal{F}\left[E_z(r_a,\phi)\right]\frac{H_n^{(2)}(\beta r_b)}{H_n^{(2)}(\beta r_a)}\right\} \tag{2.3}$$

This particular approach considers a 1D situation (only angular variations are considered) but the method nevertheless remains applicable to problems exhibiting cylindrical symmetry and provides useful insight into high frequency pattern measurement.

In [29], the radiation determination from phaseless near-field data measurements collected over limited planar surfaces (domain Ω) is approached as a non-linear inverse problem. The functional to minimize takes the form,

$$\Phi(E) = \left\| \Pi E|^2 - M_1^2 \right\|^2 + \left\| \Pi T E|^2 - M_2^2 \right\| \tag{2.4}$$

Where E is the unknown complex field tangential component over the measuring surface, M_1 and M_2 are the available square amplitudes over the corresponding surfaces and T is a linear operator connecting M_1 to M_2. The truncation operator values of Π are defined as 1

for the measurements belonging to the limited domain Ω, and 0 otherwise. The plane wave simplification,

$$E(x,y,d) = \int \hat{E}(u,v)e^{-j(ux+vy)}e^{-jwd}dudv \tag{2.5}$$

can be expanded as,

$$\begin{aligned} E &= \int \sum_{n} \sum_{m} \hat{E}_{nm} \mathrm{sinc}(au - n\pi)\mathrm{sinc}(by - m\pi)e^{-j(ux+vy)}e^{-jwd} \\ &= \sum_{-N}^{N} n \sum_{-M}^{M} m\hat{E}_{nm}\Psi_{nm}(x,y) \end{aligned} \tag{2.6}$$

since the spectrum of a planar source is a bandlimited function. Also, $u = \beta\sin\theta\cos\phi$, $v = \beta\sin\theta\sin\phi$ and $w = (\beta^2 - u^2 - v^2)^{1/2}$. The T operator in equation (2.4) can be evaluated by applying FFT or DFT methods. The values of n and m in equation (2.6) depend on any *a priori* information about the radiating source, such as for example, focusing behavior. Good simulation results were obtained, prompting the authors to conclude that by appropriately selecting the algorithms and computational techniques, it is possible to reduce the complexity of the hardware required for near-field, high frequency testing.

In [1] a new phaseless technique is introduced and the associated difficulties analyzed. The far-field distribution is included in the functional to be minimized in either of the two formulations,

$$\Phi(E) = \left\| \left| (T_1^{-1}E) \right| - M_1 \right\|^2 + \left\| \left| (T_2^{-1}E) \right| - M_2 \right\|^2 \tag{2.7}$$

where E is the generic far-field and T are the functions relating the near-field to the far-field over both measuring surfaces respectively and $M_{1,2}$ are the amplitude measurements only. The second functional,

$$\Psi(E) = \left\| E - T_1 M_1 \right\|^2 + \left\| E - T_2 M_2 \right\|^2 \tag{2.8}$$

has its variables defined in a similar way.

A procedure employed in order for the solution of minimization of either equations (2.7) or (2.8) not to be trapped in secondary minima is devised based on

inclusion of any prior knowledge of the far-field such as its focused nature and its effective bandwidth. if such information is present, even if it is only approximate, it will help to characterize the set of possible solutions by providing a search path.

The far-field is first expanded into a sampling series with a controlling parameter *N*, or the number of samples that defines the accuracy in the series. The number of local minima is obviously dependent on this number. In light of this observation, an iterative procedure is implemented, where a small *N* value will provide a guess for the initial iteration cycle, its value being slowly increased until an acceptable reconstruction of the radiated field occurs. With a sufficiently small starting value for N, the recovery will not be trapped, but the series still has to be a reasonable approximation to the field in order for the iteration process to be close to the attraction zone of the absolute minimum.

The results are validated by a plane scanning simulation where the authors found that increasing the distance between the two scanning surfaces, decreases the amount of the information about the approximate phase distribution needed to avoid optimization traps, up to a point where if the distance is large enough, no extra information should be needed.

2.3 Electromagnetic Field Interpolation

Study of digital signal processing specifies very clearly the constraints on the reconstruction of band- or time-limited signals. Applied to the field of electromagnetics, the sampling of the radiated field under certain assumptions and its subsequent reconstruction, is feasible within tolerable error bounds, and presents new desirable and useful qualities for field qualification and interpolation [6].

The required number of samples to reconstruct the radiated field are directly dependent on the Nyquist' sampling rate. The aliasing problem occurring in the event of under-sampling will preclude the proper field reconstruction since for different sampling points we would obtain different field distributions.

Methods based on the use of sampling functions for the interpolation of the near-zone radiated fields have been successfully applied for several types of radiating systems [12]. In those instances, the radiated field is approximated by interpolating functions which are quasi-bandlimited or whose effective bandwidth is in close relation to the dimensions of scattering system.

A method allowing fast analysis of radiation properties of large antennas is presented [42]. The radiated far-field is first computed with conventional techniques, in well defined spatial directions, approximately one sample for every lobe. The complete radiation pattern is then reconstructed using sampling theory.

The reconstruction of the field uses interpolation functions (reconstruction kernels), all of which display band-limited properties in their Fourrier transform domain. This is the case for the most common interpolation function, the *sinc* function defined as *sin(x)/x* (also known as cardinal series). This function and its reconstruction properties have been widely studied, and its deficiencies assessed: it has no finite impulse response, its calculation needs the evaluation of a transcendental sine function and most importantly, it decreases very slowly necessitating a large number of samples, or if a limited number of such samples is available, the result will suffer from large truncation errors. Table 1 summarizes other available bandlimited functions taken from the area of signal processing [13]. Notice that those functions can be represented as g(s) = sinc(πs/h)·ψ(s) where ψ(s) will determine the transition characteristics of the sampling expansion functions. The functions are parametrized to a variable *s*, which represents the surface of observation, either planar, cylindrical or spherical. We define the following parameters as,

$$v = \frac{\chi - 1}{\chi}, \quad m = Int\left[\frac{\pi v (N-1)}{2W}\right] + 1 \tag{2.9}$$

where χ is a number between 1 and $\sqrt{2}$ that controls the extra bandwidth W, h is defined as $\frac{\pi}{\chi W}$, and N defines the number of retained samples. Since we are interested by the

case of spherical geometry, the interpolation functions have to be applied twice, that is in the axial and azimuthal direction.

$\Psi(s)=1$	cardinal series
$\Psi(s)=\left[\operatorname{sinc}\left(\frac{v\pi s}{hm}\right)\right]^m$	self-truncating (ST)
$\Psi(s)=\frac{\sinh\left[\frac{\pi v(N-1)}{2}\sqrt{1-\left(\frac{2s}{(N-1)h}\right)^2}\right]}{\sinh\left[\frac{\pi v(N-1)}{2}\right]\sqrt{1-\left(\frac{2s}{(N-1)h}\right)^2}}$	approximate prolate (AP)
$\Psi(s)=\frac{\cosh\left[\frac{\pi vN}{2}\sqrt{1-\left(\frac{2s}{Nh}\right)^2}\right]}{\cosh\left[-\frac{\pi vN}{2}\right]}$	sampling window (SW)

Table 1- Reconstruction functions

The Fourrier-transform of the above kernels has the form,

$$g(s)\longrightarrow G(v)=\begin{cases}\frac{1}{\sqrt{2\pi}}, & |v|\le\pi-\delta\\ sm(v), & \pi-\delta<|v|\le\pi+\delta\\ 0, & |v|>\pi+\delta\end{cases} \qquad (2.10)$$

where sm(v) is used to smooth out the jump of rect(v) at $v=\pi$. The function Ψ(s) controls therefore the rate of decay of g(s).

2.3.1 Spherical Optimal Series Expansion

The optimum set of Ψ_m(s) that minimizes the incurred error in spherical coordinates has been studied in [14], and two new weighting terms are found to be producing very accurate results with limited number of samples, both with and without

the presence of relative and absolute errors in the amplitude and phase samples. Table 2 presents those functions parametrized to a circumference. and where φ_0 is the extent of the sampling domain.

$\Psi(s) = \dfrac{T_N\left[2\left(\dfrac{\cos(\frac{\varphi}{2})}{\cos(\frac{\varphi_0}{2})}\right)^2 - 1\right]}{T_N\left[\dfrac{2}{\cos^2(\frac{\varphi_0}{2})} - 1\right]}$	Tschebyscheff sampling (TS). where TN is the Tschebyscheff polynomial of degree N.
$\Psi(\varphi) = \Psi_N(\varphi.\varphi_0) = \dfrac{R_N(\varphi.\varphi_0)}{R_N(\varphi.\varphi_0)}$ *where* $R_N = \dfrac{\sinh\left[(2N+1)\sinh^{-1}\sqrt{\sin^2(\varphi_0/2) - \sin^2(\varphi/2)}\right]}{\sqrt{\sin^2(\varphi_0/2) - \sin^2(\varphi/2)}}$	Discrete approximate prolate spheroidal (DAPS).

Table 2- Optimal spherical reconstruction functions

The accuracy obtained by using either of the functions of tables 1 and 2, depends on three main points,

- sampling point position
- sampling expansion function
- number of retained samples

The choice of the function therefore has to be considered in light of the trade-off between achieved accuracy with a given number of samples and computational difficulty. In most cases, retaining extra samples and using simpler expansion functions will produce acceptable results far more rapidly than lowering the number of samples and using a more elaborate expansion function.

2.3.2 Sampling Considerations

The series expansions presented in tables 1 and 2, require *uniform* sampling. In some applications however, the exact position of the measuring probe cannot be accurately controlled. High-frequency field measurement is one of such applications. The recourse employed is to use an optical measurement system from which accurate information about the position can be obtained. The sampling grid will obviously be non-uniform, and it is of interest to know whether interpolating techniques can still be applied.

In [9] an algorithm is presented that allows interpolation from non-uniform samples. The general result obtained can be stressed as follows: for an average sampling rate equal to the Nyquist' rate, the sapling lattice must be close to a uniform one, but for a sampling rate greater than the minimum the sampling lattice can be quite arbitrary. From a computational point of view, a uniform sampling grid is first recovered from the non-uniform one before an interpolation formula is applied.

The proposed approach has been tested for stability by addition of random measurement errors, and rapidly converging results have been reported [9].

2.3.3 Band-Limited Reconstruction Kernels

Another interesting approach is to specify the expansion functions in terms of bandlimited expansion functions [2]. The functions g(*s*) specified in Tables 1 and 2 decay exponentially at best implying that for a very accurate reconstruction of a signal, the number of required samples and its associated truncation error are dependent on the sampling rate and can rapidly become large for effective computation [2]. Implementation of time (or band) limited reconstruction functions circumvents those shortcomings. To compare the two approaches, the reconstruction formulations are presented as,

$$f(t) = \lim_{W \to \infty} \sum_{k=-\infty}^{k=\infty} f\left(\frac{k}{W}\right) K(Wt - k) \qquad (2.11)$$

and,

$$f(t) = \lim_{W \to \infty} \sum_{k=\lfloor Wt-T \rfloor+1}^{k=\lfloor Wt+T \rfloor} f\left(\frac{k}{W}\right) K(Wt-k) \tag{2.12}$$

for the case of the band unlimited and band-limited case respectively. The function K is the reconstruction kernel with a limit of T in the second case, and the f function is the reconstructed signal. In the second case to reconstruct the signal f, we need exactly [2T] samples, avoiding the truncation error. Additional constraints on the time-limited reconstruction kernel to insure proper interpolation, is that its Fourrier transform be a good approximation (in some predefined sense) of the low-pass function. To further insure the smoothness of the interpolation, imposed constraints will require the Fourrier transform to be equal to *rect(x)* up to the *m*-th derivative. The approximation error can be decreased in either of the two ways; by increasing the sampling frequency W or decrease the cut-off frequency of the sampled signal. For the proposed electromagnetic application, the sampling frequency will be increased with decreased $\Delta\theta$ and $\Delta\phi$ steps, while from accuracy considerations the second means should not be used.

The reconstruction function K can be found by various methods. To insure computational efficiency the method suggested in [2] is to use the well known *B-splines*. A good explanation of B-splines is found in [3] and for the sake of completeness, the formulas to obtain them recursively are presented here as,

$$\begin{aligned} B_1 &= \begin{cases} 1, |x| \le 0.5 \\ 0, |x| > 0.5 \end{cases} \\ B_n &= B_{n-1} \cdot B_1 \end{aligned} \tag{2.13}$$

where we notice that B_n is *(n-2)* times differentiable and a time (band) limit of *n/2*. The results of interpolation simulation point in a convincing way that the usage of band-limited reconstruction kernels produces good results as compared to the truncated version of classical kernels when only a limited number of samples is available.

A method of 3D curve matching using splines presented in [4] is another potential method for field characterization to be used in lieu of methods based on reconstruction from the knowledge of sample values. This point however, will not be pursued further.

Chapter 3

Near-Field to Far-Field Transformation and Reconstruction

3.1 Introduction

Before the proposed method of phaseless near- to far-field transformation is introduced, it is advantageous to review the underlying principles on which it is based.

Firstly, the concept of the uniqueness of the radiated field is explained. As was mentioned in Chapter 2, most near- to far-field transformation methods are based on this concept. Accordingly, the present method requires the knowledge of the tangential field distribution, and uses the radial distribution in the phase retrieval procedure as additional information. Since both the amplitude and phase are necessary to uniquely represent a radiated field, we are required to retrieve the information contained in the phase distribution. The phase retrieval problem is far from being trivial, in fact it constitutes the highest hurdle in the phaseless transformations. The validity of the retrieved phase has to be assessed in the light of the difficulty to prove the uniqueness of the attained solution. Another important problem is the high possibility of convergence of the solution to local minima, an undesirable outcome.

The uniqueness theorem describes the sufficient and necessary conditions to predict the radiated field, but does not provide a method to do so. There is therefore a need for techniques that put into practical use the results of this theorem. For the proposed method, the extra constraint on the near- to far-field transformation method, is the requirement that field values be readily predicted at any distance from the first measuring surface[1]. This requirement stems from the fact that we need to find a relation, or transformation function between the measures on the first surface and field parameters

[1] this sphere encloses all inhomogeneities.

on the second. The wealth of publications on the subject (see Chapter 2) is used as starting point, and a method most suitable for phaseless implementation will be retained.

This relation can take various forms: *point-to-point*, whereby we have as many points on the first surface as we have on the second, or preferably a *many-to-one* relation. Note that the chosen relation will actually determine the complexity of the problem domain, and thus whether or not the solution is attained efficiently, if at all. When considering the amplitude field distribution only, we notice that it has a *spatial bandwidth* for all practical purposes. It is therefore desirable from an efficiency point of view, to measure solely the required number of samples, and subsequently, reconstruct the original radiated field by using common DSP techniques. Those samples would be sufficient to properly reconstruct the field and present an important reduction in the amount of necessary computations. The reconstruction functions (or kernels) as employed to this end, are of great importance to the overall accuracy. Some functions are quite simple, yet introduce a large truncation error. The most desirable kernels are those that introduce the least amount of error while reconstructing from limited number of samples. The field reconstruction theory allows us to make an assumption about the wide availability of the electromagnetic fields. This realization is important in view of practical limitations involved with the physical data measurement and not in the theoretical case adopted in this thesis. The insight gained by analyzing the properties of the scattered field can nonetheless be applied with different purpose as will be apparent in Chapter 4.

3.2 Time Harmonic Fields

Solving electromagnetic boundary-value problems entails the usage of either the Maxwell's equations or wave equations. Maxwell's equations are coupled partial differential equations, which means that they depend on both the electric and magnetic components. In order to decouple those equations, the order of the differential equation is raised: we now have second order differential *wave* equations. The electric and magnetic fields of boundary-value problems can thus be obtained by solving either the Maxwell's

or wave equations, the choice being dependent on the problem itself. The following sections present the uncoupled or wave equations used in this dissertation.

Time Varying Fields

The electric and magnetic fields can be written respectively as [15],

$$\nabla^2 \mathcal{E} = \nabla \times \mathcal{M}_i + \mu \frac{\partial \mathcal{J}_i}{\partial t} + \frac{1}{\varepsilon} \nabla q_{m} + \mu\varepsilon \frac{\partial^2 \mathcal{E}}{\partial t^2} \tag{3.1}$$

and,

$$\nabla^2 \mathcal{H} = -\nabla \times \mathcal{J}_i + \sigma \mathcal{M}_i + \varepsilon \frac{\partial \mathcal{M}_i}{\partial t} + \mu\sigma \frac{\partial \mathcal{H}}{\partial t} + \frac{1}{\mu} \nabla q_{m} + \mu\varepsilon \frac{\partial^2 \mathcal{H}}{\partial t^2} \tag{3.2}$$

For source-free regions ($J_i = q_{ev} = 0$ and $M_i = q_{mv} = 0$) and lossless media $\sigma = 0$, the equations (3.1) and (3.2) reduce to,

$$\nabla^2 \mathcal{E} = \mu\varepsilon \frac{\partial^2 \mathcal{E}}{\partial t^2} \tag{3.3}$$

$$\nabla^2 \mathcal{H} = \mu\varepsilon \frac{\partial^2 \mathcal{H}}{\partial t^2} \tag{3.4}$$

respectively. Those are the simplest form of time-varying vector wave equations.

Time Harmonic Fields

Maxwell's (wave) equations hold for an arbitrary time-dependence. The specific type of time functions that the field quantities are related to, depend on the source functions (charge density and current density). Since Maxwell's equations of interest are linear differential equations, sinusoidal time variations of source functions at some frequency will produce the same frequency variation of the field components in the steady state. It is therefore desirable to implicitly assume a time-dependence, and proceed with field calculations without any time-dependence functions as in equations (3.1) and (3.2).

Making the substitution $\partial/\partial t \Leftrightarrow j\omega$. $\partial^2/\partial t^2 \Leftrightarrow -\omega^2$ and replacing the instantaneous fields $\mathcal{E}, \mathcal{H}$ by **E** and **H** respectively in equations (3.3) and (3.4) we obtain.

$$\nabla^2 E = -\omega^2 \mu\varepsilon E \tag{3.5}$$

$$\nabla^2 H = -\omega^2 \mu\varepsilon H \tag{3.6}$$

where we define $\beta^2 = \omega^2\mu\varepsilon$. Equations (3.5) and (3.6) are the time-harmonic (time-dependence of $e^{-j\omega t}$ is implicitly assumed) for source-free and lossless media.

3.3 Uniqueness Theorem

With the uniqueness theorem [15] we state that once the complex tangential field is known on or outside an (imaginary) surface encompassing all sources, the field produced by those sources anywhere outside this (imaginary) surface is unique. We are therefore assured that by proper measurement of the tangential field distribution in the near-field of a radiator and, should a suitable transform exist, a unique radiated far-field can be predicted.

The proof for the uniqueness of the radiated field proceeds as follows: given the electric and magnetic sources $\mathbf{J_i}$ and $\mathbf{M_i}$, a lossy medium of complex constitutive parameters ε_c and μ_c within a region *S*, assume that different fields $\mathbf{E^a}$, $\mathbf{H^a}$ and $\mathbf{E^b}$, $\mathbf{H^b}$ are produced. Those fields must satisfy the Maxwell's equations,

$$-\nabla \times \mathbf{E^a} = \mathbf{M_i} + j\omega\mu_c \mathbf{H^a} \tag{3.7}$$

$$-\nabla \times \mathbf{E^b} = \mathbf{M_i} + j\omega\mu_c \mathbf{H^b} \tag{3.8}$$

$$\nabla \times \mathbf{H^a} = \mathbf{J_i} + \mathbf{J_c^a} + j\omega\varepsilon_c \mathbf{E^a} \tag{3.9}$$

$$\nabla \times \mathbf{H^b} = \mathbf{J_i} + \mathbf{J_c^b} + j\omega\varepsilon_c \mathbf{E^b} \tag{3.10}$$

subtracting (3.8) from (3.7) and (3.10) from (3.9) we obtain,

$$-\nabla \times (\mathbf{E^a} - \mathbf{E^b}) = j\omega\mu_c (\mathbf{H^a} \times \mathbf{H^b}) = \delta\mathbf{M_i} \tag{3.11}$$

$$\nabla \times (\mathbf{H}^a - \mathbf{H}^b) = (\sigma + j\omega\varepsilon_c)(\mathbf{E}^a - \mathbf{E}^b) = \delta \mathbf{J}_t \tag{3.12}$$

where J_c is the conduction electric current density in amperes per square meter.

Setting $(\mathbf{E}^a - \mathbf{E}^b) = \delta\mathbf{E}$ and $(\mathbf{H}^a - \mathbf{H}^b) = \delta\mathbf{H}$, the conditions for uniqueness are those for which $\delta\mathbf{E} = \delta\mathbf{H} = 0$. Applying the energy conservation equation with a boundary S and for time-harmonic field,

$$\oiint_S \bar{E} \times \bar{H}^* \cdot d\bar{s} + \iiint_V \left(\bar{E} \cdot \bar{J}_t^* + \bar{H}^* \cdot \bar{M}_t \right) dv = 0 \tag{3.13}$$

and in our case,

$$\oiint_S \left(\delta\bar{E} \times \delta\bar{H}^* \right) \cdot d\bar{s} + \iiint_V \left[(\sigma + j\omega\varepsilon_c)^* \left| \delta\bar{E} \right|^2 + j\omega\mu_c \left| \delta\bar{H} \right|^2 \right] dv = 0 \tag{3.14}$$

so if we assume that the first term of the above equation is equal to zero, then the volume integral must be zero as well. Since the real parts of $(\sigma+j\omega\varepsilon_c)^*$ and $j\omega\mu_c$ are positive for dissipative media, the volume integral will be equal to zero only for $\delta\mathbf{E} = \delta\mathbf{H} = 0$, which would prove that $(\mathbf{E}^a - \mathbf{E}^b) = 0$ and $(\mathbf{H}^a - \mathbf{H}^b) = 0$ and therefore uniqueness. We now have to find the conditions under which the assumption is valid. The first term of (3.14) can also be written with the help of,

$$A \cdot (B \times C) = B \cdot (C \times A) = C \cdot (A \times B) \tag{3.15}$$

as,

$$\oiint_S \left[\delta\bar{E} \times \delta\bar{H}^* \right] \cdot \hat{n}\, da = \oiint_S \left[\hat{n} \times \delta\bar{E} \right] \cdot \delta\bar{H}^* da = \oiint_S \left[\delta\bar{H}^* \times \hat{n} \right] \cdot \delta\bar{E}\, da = 0 \tag{3.16}$$

where $\hat{n}$ is the normal to the chosen surface. Thus if the tangential components of $\mathbf{H}$ over a boundary (or closed imaginary surface) are known ($\hat{n} \times \bar{H}$), and equation (3.16) holds, then this is the necessary and sufficient information to predict the field at any other point outside this boundary or surface.

Similarly, uniqueness also holds for the following cases,

- tangential components of $\mathbf{E}$ are known over the boundary,

- tangential components of **E** are known over part of boundary and tangential components of **H** are known over the rest of the boundary.

Note also that lossless media, as assumed in this dissertation, can be treated as a special case of dissipative media as the losses decrease.

The uniqueness theorem proves that if either of the three conditions specified above is met, it is a sufficient condition to calculate the radiated field anywhere outside the region S, but it does not yield any insight as to how to carry out those calculations.

3.4 Near- to Far-Field Transformation Methods

Most methods are applicable for a wide variety of EMI/EMC testing procedures and antenna characterization. All methods are implemented numerically and assume a homogeneous space which greatly simplify the theoretical part of a transform. The following presents two methods considered for the proposed implementation. Upon further reflection and trials, the first method was rejected due to the conjectured negative impact of the presence of field derivatives on the phase retrieval algorithm while keeping all other things equal.

3.4.1 Exact Integral Equation Method

In the formulation presented in [10], using Green's second identity for vector fields,

$$\begin{aligned}&\int_V \left(\bar{Q}\cdot\nabla\times\nabla\times\bar{P}-\bar{P}\cdot\nabla\times\nabla\times\bar{Q}\right)dV = \\ &\oint_{S=S_1\cup S_2}\left(\bar{P}\times\nabla\times\bar{Q}-\bar{Q}\times\nabla\times\bar{P}\right)\cdot d\bar{S}\end{aligned} \tag{3.17}$$

in which $\bar{P}$ is replaced by electric or magnetic field, $\bar{Q}$ by the Green's homogeneous function,

$$\bar{Q}=\hat{a}\phi(\bar{r},\bar{r}')=\hat{a}\frac{e^{-j\beta|\bar{r}-\bar{r}'|}}{|\bar{r}-\bar{r}'|} \tag{3.18}$$

S_1 and S_2 are the surface enclosing all sources and the surface at infinity respectively. The integral in (3.17) reduces to an integral over S_1 and after extensive manipulation the relation between the field outside the surface enclosing all sources and the field on this surface is for the magnetic field,

$$\bar{H}(\bar{r}) = \frac{1}{4\pi}\int_{S_1}\left[\bar{H}(\bar{r})\frac{\partial\phi(\bar{r},\bar{r}')}{\partial n'} - \phi(\bar{r},\bar{r}')\frac{\partial\bar{H}(\bar{r})}{\partial n'}\right]dS \qquad (3.19)$$

whence the following restrictions apply,

- the surface S_1 encloses all inhomogeneities,
- the primed coordinate system is for the surface S_1,
- the observation point $\bar{r}$ cannot lie on the surface S_1,
- there are no incident fields.

While this method provides good results [10] when the phase is readily available, it has been rejected in favor of the spherical wave expansion method for reasons that will become apparent in the next section.

3.4.2 Spherical Wave Expansion

Electromagnetic fields associated with a given boundary value problem must satisfy Maxwell's equations or the vector wave equations. In the present case, the vector wave equations reduce to three scalar Helmholtz wave equations and the general solution is composed of the solution to each of the scalar wave equations.

The properties of the spherical waves, the solution to the homogeneous system of equation are developed in various papers [24].

Spherical Wave Solution

Starting with,

$$\nabla^2\Psi(r,\theta,\phi)=-\beta^2\Psi(r,\theta,\phi) \tag{3.20}$$

where $\Psi(r,\theta,\phi)=f(r)g(\theta)h(\phi)$ is the vector potential component, and after some manipulation we obtain three scalar differential equations.

$$\frac{d}{dr}\left\{r^2\frac{df(r)}{dr}\right\}+\left\{(\beta r)^2-n(n+1)\right\}f(r)=0 \tag{3.21}$$

$$\frac{1}{\sin\theta}\frac{d}{d\theta}\left\{\sin\theta\frac{dg(\theta)}{d\theta}\right\}+\left\{n(n+1)-\left(\frac{m}{\sin\theta}\right)^2\right\}g(\theta)=0 \tag{3.22}$$

$$\frac{d^2h(\phi)}{d\phi^2}=-m^2h(\phi) \tag{3.23}$$

where m and n are usually integers.

Note that the equation (3.21) has the form of the Bessel differential equation,

$$x^2\frac{d^2y}{dx^2}+x\frac{dy}{dx}+\left(x^2-p^2\right)y=0 \tag{3.24}$$

and it has for solutions,

$$y(x)=A_1J_n(x)+B_1Y_n(x) \tag{3.25}$$

$$y(x)=C_1h_n^{(1)}(x)+D_1h_n^{(2)}(x) \tag{3.26}$$

where $J_n(x)$ and $Y_n(x)$ are the Bessel function of the first kind and second kind respectively, and $h_n(x)$ are the Hankel functions.

The equation (3.22) resembles the Legendre differential equation,

$$\left(1-x^2\right)\frac{d^2y}{dx^2}-2x\frac{dy}{dx}+\left[n(n+1)-\frac{m^2}{1-x^2}\right]y=0 \tag{3.27}$$

The solution of the differential equation (3.27) is composed of the associated Legendre functions of the first and second kind respectively,

$$y(x) = A_2 P_n^m(x) + B_2 P_n^m(-x) \qquad n \neq integer \tag{3.28}$$

or,

$$y(x) = C_2 P_n^m(x) + D_2 Q_n^m(x) \qquad n = integer \tag{3.29}$$

where $P_n^m(x) = 0$ for $m > n$.

The (3.23) equation will have for solution.

$$h(\phi) = A_3 e^{-jm\phi} + B_3 e^{jm\phi} \tag{3.30}$$

or,

$$h(\phi) = C_3 \cos(m\phi) + D_3 \sin(m\phi) \tag{3.31}$$

The solution to (3.20) will be the product of the solutions to (3.21), (3.22) and (3.23), which in turn depend on the exact specification of the problem. For outward propagating waves, as is clearly required in our case (obtaining far-field measures from near-field ones) the general solution will be the product of (3.26) (3.29) and (3.31),

$$\begin{aligned} \Psi(r,\theta,\phi) = &\left[C_1 h_n^{(1)}(\beta r) + D_1 h_n^{(2)}(\beta r)\right] \times \\ &\left[C_2 P_n^m(\cos\theta) + D_2 Q_n^m(\cos\theta)\right]\left[C_3 \cos(m\phi) + D_3 \sin(m\phi)\right] \end{aligned} \tag{3.32}$$

Extension to Electromagnetic Fields

The equation (3.32) is used to obtain the solution for the vector potentials satisfying both,

$$\nabla^2 A + \beta^2 A = -\mu J \tag{3.33}$$

$$\nabla^2 F + \beta^2 F = -\varepsilon M \tag{3.34}$$

where J and M are set to zero due to the homogeneity assumption. The total electric and magnetic fields are obtained by superposition of the individual fields due to A and F,

$$E = -j\omega A - \frac{j}{\omega\mu\varepsilon}\nabla(\nabla \cdot A) - \frac{\nabla \times F}{\varepsilon} \tag{3.35}$$

$$H = -j\omega F - \frac{j}{\omega\mu\varepsilon}\nabla(\nabla \cdot F) + \frac{\nabla \times A}{\mu} \tag{3.36}$$

The complete solution will be described by the field configuration produced by the *transverse electric* and *transverse magnetic modes* $\mathbf{TE}^r$ and $\mathbf{TM}^r$ respectively. The TE modes are found by setting A=0 and $F = \hat{r}F(r,\theta,\phi)$, for the TM modes the situation is reversed, $F = 0$, and $A = \hat{r}A(r,\theta,\phi)$. The complete solution necessitates the determination of the coefficients that depend on the boundary conditions.

Boundary constraints

The boundary conditions that must be satisfied are,

$$E_\theta(r = a, 0 \le \theta \le \pi, 0 \le \phi \le 2\pi) = E_\theta^s \tag{3.37}$$

$$E_\phi(r = a, 0 \le \theta \le \pi, 0 \le \phi \le 2\pi) = E_\phi^s \tag{3.38}$$

$$E_\theta(r = \infty, 0 \le \theta \le \pi, 0 \le \phi \le 2\pi) = 0 \tag{3.39}$$

$$E_\phi(r = \infty, 0 \le \theta \le \pi, 0 \le \phi \le 2\pi) = 0 \tag{3.40}$$

where a is the radius of the imaginary surface enclosing all inhomogeneities and $\mathbf{E}^s$ are the electric field samples taken on this surface.

Applying the boundary conditions we find that the associated Legendre polynomials of the first kind and spherical Besel functions are necessary to describe the spherical wave solution. Moreover, in order to satisfy the radiation condition at infinity, the spherical Besel functions are restricted to spherical Hankel functions of the second kind,

- C_1 is equal to zero since it represents *inward* propagating waves,

- D_2 is equal to zero since the field is finite at $\theta = 0,\pi$ and $Q_n^m(\cos\theta)$ presents a singularity at those points.

which yields the following equation,

$$\Psi(r,\theta,\phi) = B_{mn} h_n^{(2)}(\beta r) P_n^m(\cos\theta)\left[C_3\cos(m\phi) + D_3\sin(m\phi)\right] \tag{3.41}$$

where the remaining coefficients depend on the values of the boundary conditions. For the case of tangential electric field known upon a surface the derivations are performed in [17] and the results are presented in the next section.

Solution of Maxwell's equations

The solutions to the homogeneous vector-wave equations in spherical coordinates is expressed by defining M_{mn} and N_{mn} as:

$$\begin{aligned} M_{mn} = \mp z_n(k\rho)\frac{mP_n^m(\cos\theta)}{\sin\theta}\begin{bmatrix}\sin\\ \cos\end{bmatrix}(m\phi)\bar{\theta} \\ - z_n(k\rho)\frac{\partial}{\partial\theta}P_n^m(\cos\theta)\begin{bmatrix}\cos\\ \sin\end{bmatrix}(m\phi)\bar{\phi} \end{aligned} \tag{3.42}$$

$$\begin{aligned} N_{mn} = n(n+1)\frac{z_n(k\rho)}{k\rho}P_n^m(\cos\theta)\begin{bmatrix}\sin\\ \cos\end{bmatrix}(m\phi)\bar{\rho} \\ + \frac{1}{k\rho}\frac{\partial}{\partial\rho}\left[\rho z_n(k\rho)\right]\frac{\partial}{\partial\theta}P_n^m(\cos\theta)\begin{bmatrix}\sin\\ \cos\end{bmatrix}(m\phi)\bar{\theta} \\ \pm\frac{1}{k\rho}\frac{\partial}{\partial\rho}\left[\rho z_n(k\rho)\right]\frac{mP_n^m(\cos\theta)}{\sin\theta}\begin{bmatrix}\cos\\ \sin\end{bmatrix}(m\phi)\bar{\phi} \end{aligned} \tag{3.43}$$

where the time dependence is implicitly assumed. The two functions are the transverse electric (TE) and transverse magnetic (TM) waves where we note the presence of even an odd modes (upper or lower sin dependence). The coefficients of the wave functions are,

$$a_{mn} = \frac{1}{\left[z_n(k\rho_1)\right]^2}\frac{2n+1}{\pi 2n(n+1)}\frac{(n-m)!}{(n+m)!}\cdot \int_0^{2\pi}\int_0^{\pi} M_{mn}\cdot E(\rho_1,\theta,\phi)_{tan}\sin\theta d\theta d\phi \tag{3.44}$$

$$b_{mn} = \frac{1}{\left[(1/k\rho_1)(\partial/\partial\rho_1)\left[\rho_1 z_n(k\rho_1)\right]\right]^2}\cdot \frac{2n+1}{\pi 2n(n+1)}\frac{(n-m)!}{(n+m)!}\int_0^{2\pi}\int_0^{\pi} N_{mn}\cdot E(\rho_1,\theta,\phi)_{tan}\sin\theta d\theta d\phi \tag{3.45}$$

where $0 < \rho < \rho_1 < \infty$. In terms of the spherical wave functions M_{mn} and N_{mn}, and their coefficients the fields for $\rho < \rho_1$ can be expressed as a summation:

$$E(\rho,\theta,\phi) = -\sum_m \sum_n a_{mn}M_{mn} + b_{mn}N_{mn} \tag{3.46}$$

$$H(\rho,\theta,\phi) = (k/j\omega\mu)\sum_m \sum_n a_{mn}N_{mn} + b_{mn}M_{mn} \tag{3.47}$$

Since all sources were defined to be within the sphere of radius ρ, spherical waves of order $n>k\rho$ will not contribute significantly to the field [18]. Due to constraints on axial radiation [19], the value of m is limited to 1. Also, because of the properties of the associated Legendre functions, $m \le n$.

Of practical interest are asymptotic approximations to the spherical Hankel functions $h_n^{(2)}(k\rho)$, in the far-field region,

for $k\rho > n^2$

$$h_n^{(2)}(k\rho) \equiv (j)^{n+1}\frac{e^{-jk\rho}}{k\rho}$$
$$\frac{1}{k\rho}\frac{\partial}{\partial\rho}\left(\rho h_n^{(2)}(k\rho)\right) \equiv j^n\frac{e^{-jk\rho}}{k\rho} \tag{3.48}$$

which result in much simplified calculations when considering only calculations in the far-field.

3.5 Analytical Properties of the Scattered Field

The analysis of the scattered fields can give us great insight into the behavior of electromagnetic waves from perspective other than the usual Maxwell's or wave propagation will. Since upon implementation we will work with field samples, it is obviously of interest to investigate what impact it will have on the formulation developed above. The primordial goal is to be able to describe the radiated field in a way that lends itself to digital manipulation.

Spatial Bandwidth of Scattered Fields

The radiated field is not a bandlimited function in a strictly mathematical sense. From analysis, however, it is evident that a very sharp transition in error occurs when using bandlimited function to reconstruct the original field: at a critical point this error changes from important to negligible, thus the concept of effective (spatial) bandwidth.

We represent the scattered field as,

$$E_0(r) = \int_D G_0(r,r')J(r')dr' \qquad (3.49)$$

where $\mathbf{J(r')}$ is the current density, $\mathbf{r}$ is the vector from the origin of the coordinate system to the observation point and $\mathbf{r'}$ is the vector from the origin to the radiating element position as depicted in Figure 2.

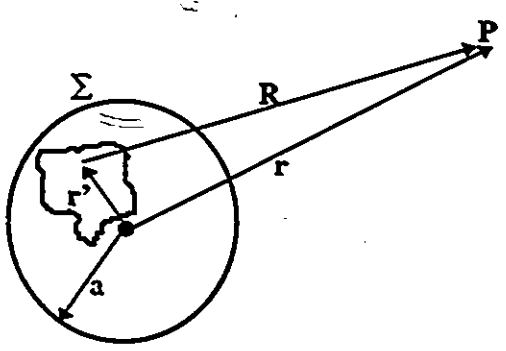

Figure 2 Geometrical specifications

and $\mathbf{G_0(r,r')}$ is the free-space Green's function.

$$\bar{G}(r,r') = -j\frac{\omega\mu}{4\pi|\bar{r}-\bar{r}'|}e^{j\beta(r-|r-r'|)}\bar{N}(\bar{r}-\bar{r}')$$
$$\bar{N}(r,r') = \bar{I} + |\bar{r}-\bar{r}'|e^{j\beta|r-r'|}\frac{\nabla\nabla}{\beta^2}\frac{e^{-j\beta|r-r'|}}{|\bar{r}-\bar{r}'|} \tag{3.50}$$

factoring out the phase dependence $e^{(-j\beta r)}$ from the equation (3.49),

$$E(r) = E_0(r)e^{j\beta r} \tag{3.51}$$

The new function becomes,

$$E(r) = \int_D G(r,r')J(r')dr' \tag{3.52}$$

which is then projected onto some set of bandlimited functions Γ_w producing $\mathbf{E_w(r)}$. The projection is attained through a convolution operation onto a suitably chosen function. This function will depend on the observation domain, either planar or circular. Introducing a parameter *s* representing a parametrized surface, the error from such approximation is,

$$\Delta E(s) = E_w(s) - E(s) \tag{3.53}$$

This error exhibits a step-like behavior, producing a large error up to a critical value of the bandwidth, decreasing rapidly towards zero thereafter. The effective bandwidth is expressed in terms of bounding limits and depends only on the dimension of the radiating system and the frequency of operation,

$$\beta a \le W \le \sqrt{2}\beta a \tag{3.54}$$

Those bounding limits are obtained by evaluating equation (3.53), which involves asymptotic evaluation at stationary points of the integral appearing in (3.52).

Since the radiated electromagnetic field is characterized by a spatial bandwidth *W*, a set of functions bandlimited to $w = \chi W$, with $\chi > 1$, can be used to approximate the field. The maximum relative error decreases proportionally to $e^{(\chi-1)}$ and e^{W}, so for large scatterers where $\beta a >> 1$, χ has to be only slightly larger than unity. Any form of

sampling expansion functions can be used in order to optimize the reconstruction algorithm from a numerical point of view [6].

As mentioned above, appropriate observation domain parametrization is necessary and for a circular domain the bandlimited functions are periodic in $2\pi\sin\theta$. The total number of samples will be approximately equal to,

$$\frac{4}{\pi}(\chi\beta a)^2 \tag{3.55}$$

which is of the same order of that needed for spherical wave expansion. Unlike in the spherical expansion, the series can be truncated to only retain the samples near the point of interest. The coefficients of the reconstruction functions are the field values themselves and not their linear functionals (see section 3.4.2).

Three main points are recalled,

- field approximation (reconstruction) on an observation domain external to spatially bounded sources is possible by bandlimited functions,
- the incurred error possesses a step-like behavior,
- bandwidth of the scattered field depends on the source dimension.

As was shown above we can reconstruct the radiated field from a limited number of samples. The above method is an efficient and convenient way for interpolating the scattered field and not a wave expansion technique: it is a rigorous way for representing the scattered field everywhere in space starting from the knowledge of the field distribution over a surface. Similarly, if only a particular region on the measuring sphere is of interest, only samples from this region need evaluating.

Degrees of Freedom of Scattered Fields

Measurements of the radiated electromagnetic field will certainly be corrupted. The reasons affecting the minimum detectable field are: noise, system sensitivity, and measurement errors. The maximum field measurements are dependent on the dynamics of

the measuring apparatus. The spatial and temporal characteristics will determine the accuracy of the measurements. Finally, all the round-off and truncation errors have to be accounted for in all digital computations.

Due to the sum of all the imperfect parameters and generalized failure to correctly evaluate the radiated field, the actual measures will represent many mathematically distinct field distributions.

The important result is that from a practical point of view, a minimum number of independent parameters can be used to describe a given system with a specified precision. Applied to the electromagnetic field, that would mean that the knowledge of the total radiated field distribution can be replaced by the knowledge of a certain number of functions or variables. Those variables can be used henceforth in all relevant calculations and transformations in a way that maximizes the available computing power, since no redundant information is used. We can immediately see the similarity of the minimum number of the variables to the concept of information content and informational entropy [7]. The purpose of this section is to state that each radiated field has a certain associated *degrees of freedom* which completely describe its behavior with a given precision.

The bounds for the degrees of freedom are derived from the knowledge of the effective bandwidth (see previous section) which suggest the following procedure,

- a bandwidth $w = \chi_1 W_0$ is selected within the prescribed error bounds, and where $\chi_1 > 1$ and $W_0 = \beta a$ as defined in the previous section.
- a sampling rate $N = \chi_2 w/\pi$ is chosen to be within prescribed truncation error bounds.
- the field can the be reconstructed using the values at the sampling points whose spacing is given by $\pi/(\chi_1\chi_2 W_0)$.

With this procedure, the scattered electromagnetic field can be reconstructed within any preset error bounds. The reconstruction utilizes a minimal number of basis functions which uniquely define the degrees of freedom of a particular scattered field.

3.6 Phase Retrieval Problem

The phase retrieval problem has been investigated in various areas, optics, astronomy, remote sensing and holographic imaging inclusively. An extensive bibliography exists, far too extensive in fact to be included in this dissertation. A comprehensive list is included in the references of [46].

In the present dissertation, this problem arises from the fact that the knowledge of the radiated field is restricted to the amplitude distribution only, whereas the phase distribution is needed as well to fully characterize the scattered field. This can also be seen from the fact that although a unique Fourrier transform[2] exists between the far-field and the near-field, no such relation exists for the intensities of those fields. We can therefore safely state that additional information or processing of the near-field must be performed in order to obtain the phase distribution. Possible solutions to this problem depend on either the analytic properties of the fields or on a specific computational procedure dependent in one way or another on properties of the near-field. As mentioned previously, various examples can be found on methods such as reference field additions and the usage of multiple intensity distributions (reference of [46]).

Interesting development has been presented in [5] in which the author uses the Hilbert transform to relate the real and imaginary parts of causal spectral response. By applying this method a *minimum phase* function can be obtained, from which the transient response can be computed. However, this method does not guarantee the reconstruction of the actual transient response. The Hilbert transform relates the real part and the imaginary part of a function that has finite nonzero extent,

$$\mathrm{Im}(F(x)) = \mathcal{H}\,(\mathrm{Re}(F(x)) \tag{3.56}$$

so that knowing the magnitude of $F(x)$ we can apply numerical procedures and retrieve the argument of $F(x)$. However, if the function $F(x)$ has zeros (a zero is defined a number for which the function yields a result of zero) that are not on the real axis or in the lower half-plane, each will contribute a phase increment. In the other case, a function known as

[2] defined for one dimensional case

the minimum phase is obtained. The phase increments can be calculated if the location of the zeros is known, unfortunately very little information on the distribution of zeros of the entire functions of exponential type is available [46].

The knowledge of intensity distribution on both the near- and far-field surfaces does certainly contain new information that can be used for phase retrieval purposes. Similarly, amplitude information from two slightly defocused image planes yields the necessary extra information. The first approach was suggested by Gerchberg and Saxton, and the second by Misell (references are included in [46]). Both methods have been subsequently proved to produce unique solutions, if analyticity of the functions involved is assumed. Ambiguities remain for constant phase shifts and complex conjugates, the resolution of which necessitates other type of information. Those methods have been tested by other researchers with mixed success, and the correctness of the obtained result still seems to depend on the choice of initial guess, functions and number of samples.

The uniqueness of the phase recovery is based on the assumption of analyticity of the functions. In numerical procedures however, analyticity cannot be completely realized, prompting for the requirement that the near-field distribution possesses continuous first derivative - requirement that still does not generally guarantee unique retrieval.

Developments presented in [8] proposes a method of determining the relative phases among the components of an electromagnetic field at a single point from amplitude measurements only. It provides both the necessary and sufficient conditions to retrieve a unique phase. There is no extension for retrieving the relative phase between individual points, and in its present form, it is not applicable to the problem at hand.

As a conclusion to this section, let it be stated that the unique solution to the phase retrieval problem is theoretically attainable with the knowledge of amplitude distribution on more than one surface, as applicable to the method presented in this dissertation.

Chapter 4

Phaseless Near- to Far-Field Transformation

4.1 Introduction

A setup similar to the one presented in [10] will be used to gather field information on a spherical surface that encloses all inhomogeneities. This information, collected usually in the near-field of the device under test, will allow to characterize its far-field radiation pattern. In certain circumstances, such as at high operating frequencies, accurate measurement of the phase can be practically impossible to perform while those for amplitude components are comparatively much easier to obtain. Since both amplitude and phase information are necessary for proper near- to far-field transformation, a method has to be first devised for retrieving the phase distribution from the knowledge of amplitude distribution only. One such method involves measuring the amplitude distributions on two distinct spherical surfaces, and to minimize a properly chosen functional. By uniqueness theorem, the knowledge of the tangential field radiation on a surface enclosing all radiating elements is sufficient to compute the radiation anywhere on or outside a spherical surface of radius ρ_0 that includes all inhomogeneities.

Minimizing a functional is therefore a way to estimate the unknown phase distribution. Application of the spherical wave expansion method allows us to relate the two surfaces by way of superposition of spherical wave functions and their associated coefficients. The spherical wave functions depend only on the problem geometry, while the coefficients are derived from the boundary conditions, or specifically, the knowledge of tangential field distribution over the surface. By using this formulation, the problem of phase retrieval for a potentially large problem domain (phase associated to each amplitude measurement) is reduced to the estimation of expansion coefficients. The number of such coefficients is finite in extent since higher order spherical expansion

functions contribute infinitesimal amounts to the total power. In short, the actual phase distribution over a surface is not explicitly found, instead a search is performed for the spherical wave expansion function coefficients, the knowledge of which will uniquely determine the far-field radiation pattern. Since minimization of a functional is involved, an adequate method of constrained optimization has to be applied. Very important from overall performance point of view, a detailed description of the involved methods and mechanisms is beyond the scope of this thesis. Such procedures searches for those coefficients that minimize a cost function defined in terms of measured amplitudes on one surface. Further, the search is constrained to the bounds derived for each coefficient from the knowledge of the amplitudes measurements on the other surface.

The actual implementation is documented pointing to all the possible sources of error introduced in the process while results are deferred until Chapter 5.

4.2 Problem Statement

In the following, it is assumed that amplitude measurements are carried over two distinct but close together surfaces, Σ_1 and Σ_2. The measured parameter is $\mathbf{E}_{tan}$ on both surfaces. Since spherical coordinates are used throughout, $\mathbf{E}_{tan} = \mathbf{E}_\theta + \mathbf{E}_\phi$ and we get the following set of equation representing the radiated field produced by the same device:

$$E_{A\tan} = E_{A\theta}\bar{\theta} + E_{A\phi}\bar{\phi} \quad on\ surface\ \Sigma_1 \tag{4.1}$$

$$E_{B\tan} = E_{B\theta}\bar{\theta} + E_{B\phi}\bar{\phi} \quad on\ surface\ \Sigma_2 \tag{4.2}$$

and we recall that only amplitudes of $E_{A\tan}$ and $E_{B\tan}$ are known. Rewriting equations (3.44) and (3.45) for the spherical wave coefficients, a_{1n} and b_{1n},

$$a_{1n} = \frac{2\pi}{I}\frac{\pi}{J}k_{1n}\sum_{i=0}^{I}\sum_{j=0}^{J}M_{1n}(i,j)\cdot E_{A\tan}(i,j)\sin(\tfrac{i\pi}{I})$$
$$where \quad k_{1n} = \frac{1}{\left[z_n(k\rho_1)\right]^2}\frac{2n+1}{\pi 2n(n+1)}\frac{(n-1)!}{(n+1)!} \tag{4.3}$$

$$b_{1n} = \frac{2\pi}{I}\frac{\pi}{J} \cdot l_{1n} \sum_{i=0}^{I}\sum_{j=0}^{J} N_{1n}(i,j) \cdot E_{A\tan}(i,j)\sin(\tfrac{i\pi}{I})$$

$$where \quad l_{1n} = \frac{1}{\left[(1/k\rho_1)(\partial/\partial\rho_1)[\rho_1 z_n(k\rho_1)]\right]^2} \frac{2n+1}{\pi 2n(n+1)} \frac{(n-1)!}{(n+1)!} \tag{4.4}$$

and replacing in the equation (3.46).

$$E_{B\tan} = -\sum_n a_{1n} M_{1n} + b_{1n} N_{1n} \tag{4.5}$$

so any set of E_{Atan} producing equations (4.3) and (4.4) and satisfying equation (4.5) is a solution. Because only the amplitude of E_{Atan} and E_{Btan} are known, we have to minimize the function,

$$\Phi(a_{1n}, b_{1n}) = norm\left(\left\| E_{B\tan} \right\| - \left\| \sum_n a_{1n} M_{1n} + b_{1n} N_{1n} \right\| \right) \tag{4.6}$$

which will allow us to estimate the phase distribution. The $\| \ \|$ symbol represents the absolute value. In the algorithm, equation (4.6) is implemented with the euclidian norm while the minimization is performed with respect to the a_{1n} an b_{1n} variables.

From the knowledge of the magnitude and phase distribution of the electromagnetic field over a surface enclosing all radiating elements, we can obtain results for the radiated electromagnetic far-field anywhere outside the enclosing surface. From equation (4.6), it is apparent that only the (a,b) coefficients are unknown. By selecting various possible combinations of phase distribution, those coefficients can be found from equations (4.3) and (4.4). Application of equation (4.6) will then yield a nearness value of such choice. The phase is therefore found directly, and we note that the size of the problem is related to the number of amplitude samples taken. For accuracy purposes, it is obviously desirable to have as many samples as possible. An analysis of the trade-off between the accuracy of the solution and its computability is needed in order to assess the feasibility of the approach. Directing our attention back to the equation (4.6), we notice that the knowledge of the coefficients is, just as the knowledge of the phase, sufficient to predict the radiation field anywhere. A much more appropriate approach is

therefore to optimize directly for the coefficients and to use the equations (4.3) and (4.4) to derive bounds for the coefficients, restricting the search over the solution domain.

Before proceeding further, the equation (4.6) should be analyzed. E_{Btan} represents the radiated electric field on the second surface, of which only the amplitude is known. The summation involving the *TE* and *TM* modes is a linear transformation, and their respective coefficients dependent on the tangential radiated electric field as measured on the first surface. Again, only the amplitude of the tangential field is known. By assuming the phase distribution on the first surface, we will obtain some radiated field on the second surface. The functional will measure the actual nearness of the measured and inferred amplitudes. A result of zero in equation (4.6) would signify a perfect match, the most desirable and unlikely outcome. Assuming the value obtained will be close to zero, or to some pre-defined value deemed acceptable within the error bounds, what is the information that we can extract from it? Obviously the amplitudes match, but do the phases as well? If we refer to the discussion in section 3.6, we could state that theoretically the phases will match, usually with the same offset for all values. This offset can effectively be disregarded for relative notions such as phase. In practice, various initial guesses will serve as inputs to the algorithm and as will be presented in Chapter 5, reasonable convergent behavior can be expected.

Next important question to arise is the number of sample points we require to attain an acceptable result. Assume for that purpose that the samples on the first surface are readily available anywhere, as to effectively reduce the error from spherical wave expansion. This is the case in the present dissertation, as the field values are obtained through computer simulation; otherwise field interpolation techniques presented in Chapter 2 can be used to render this assumption valid. We notice here that the amplitude points on the second surface act as constraints. If we had only one point on the second surface, we could have different solutions for the phase distribution on the first surface. If we had as many or more samples on the second surface than the first, intuitively we would get only one solution. Obviously, intuition is a rather vague concept, and it needs some more formal underlying principles to state the previous assertion in a mathematical

framework. From the discussion analytical properties of the radiated fields (see section 3.5) we know that a certain number of samples is required to describe or characterize completely the radiated field within reasonable error bounds. There is a relation between this number of samples and the concept of *degrees of freedom* of scattered fields. The degrees of freedom are the minimum number of independent parameters, in our case measurements, that are needed to describe a function within the measurement accuracy. We can view this concept as expressing the radiated field in terms of *coordinates* or *basis vectors*. We can see that the two concepts, sampling and degrees of freedom, share the same requirements, and in fact both are dependent on the effective (spatial) bandwidth, and both can be approximated by the calculation of the Nyquist's number N_0. The concept of degrees of freedom is widely utilized in mechanics or in the field of robotics. If we know that a system has n degrees of freedom, specifying n independent constraints will limit the search for an extremum of a specified functional. The correct solution will still not be guaranteed since local extrema will be reduced but not eliminated altogether. This problem could be circumvented with a rough knowledge of the phase distribution obtained with some other means or some particular numerical procedure employed to avoid the secondary minima (see section 2.2). This will be dealt with in the next section.

The phase, although a natural choice, as appears from preceding discussion is not the best solution for our purpose. Rewriting equation (4.6) as to explicitly show its dependence on spherical wave coefficients,

$$\Phi(a_{1n}, b_{1n}) = norm\left(\left\| E_{B\,tan} \right\| - \left\| \begin{bmatrix} M^{\theta}_{1n} & N^{\theta}{}_{1n} \\ M^{\circ}_{1n} & N^{\circ}{}_{1n} \end{bmatrix} \begin{bmatrix} a_{1n} \\ b_{1n} \end{bmatrix} \right\| \right) \tag{4.7}$$

The minimization is therefore done with respect to the (a,b) coefficients and not the phase distribution of the first surface. Once those coefficients are known, the radiated electromagnetic field can be computed anywhere outside the surface enclosing all inhomogeneities. The size of the involved matrices is as follows. The coefficients (a,b) are column matrices with length dependent on the number of expansion modes n and the total size is $4n$ (accounting for both a and b coefficients and their respective even and odd modes). The matrix containing the *TE* and *TM* factors has for rows the number of

independent measurements on the second surface. We notice that for this matrix to be square, twice as many measurement points than number of mode expansion have to be selected. The last column matrix holds the amplitude measurements on the selected points on the second surface.

4.3 Retrieval Algorithm

Implementing equation (4.7), we note that the field distribution on the second surface will be dependent on the coefficients, calculated in turn from the field distribution on the first surface. The coefficients are the same for all three coordinate vector components when the order n is the same (eq. 4.3 and 4.4). Recalling the uniqueness theorem in section 3.3, the knowledge of tangential field components completely describes the radiated field. The minimization of the functional therefore must take into account both values at the same time. In another words, it is possible to find a phase distribution such that it would perfectly match one of the vector field components, but produce erroneous results in the remaining components. To illustrate this point, let us take a closer look at a simplified case where the minimization is done only for the θ component of the radiated field (the ϕ-directed vectors are assumed to be zero).

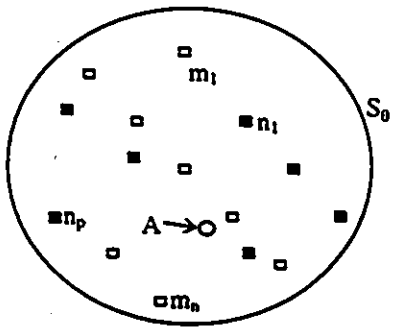

Figure 3 Solution domain of one distribution

The solution domain S_θ is defined as the solution to equation (4.6) for all possible permutations of the set $\{\theta_k\}$. The task of the minimization therefore is to find the

minimum, zero for the particular case of equation (4.6), over this k-dimensional space. Please refer to Figure 3; the point A denoted by a little circle represents the absolute minimum, or a value of zero for equation 4.6. Points m_1 through m_n denoted by little squares represent secondary minima which have to be assumed as acceptable solutions for a certain error level ε (see 3.5). Points n_1 through n_p denoted by little gray squares denote secondary minima that do not constitute a solution at an error level ε. From Figure 3 we clearly see that whether the solution will get trapped in a secondary minima depends essentially on the choice of the initial "guess" of the coefficient distribution taken from the set $\{a_n, b_n\}$. A solution that converged to one of the n points is clearly not the solution as would be apparent from *a posteriori* analysis of the solution. If the solution ends up in either the points A or m, we have to accept it as the solution. In the particular case of electromagnetic fields this will in general could be an erroneous solution since we also require the minimization to be performed over S_ϕ simultaneously. To make this example applicable (and valid) in the electromagnetic application, we add the solution domain S_ϕ as in Figure 4.

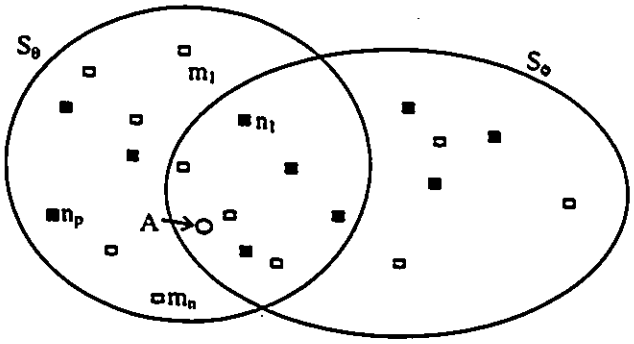

Figure 4 Solution domain for related disjoint distributions

We can notice that generally, the domains S_θ and S_ϕ can have some minima in common and some particular to their respective domains. Up to this point both domains are still disjoint. In order to join the two domains various means can be applied, the most convenient being the square root norm. In this case we obtain a new solution domain,

$$S_{tan} = f(S_\theta, S_\phi) \tag{4.8}$$

where f represents a joining function, the euclidian norm. The new distribution remains k-dimensional but whose location of extremum points will generally be different than either of S_θ or S_ϕ except for some particular cases.

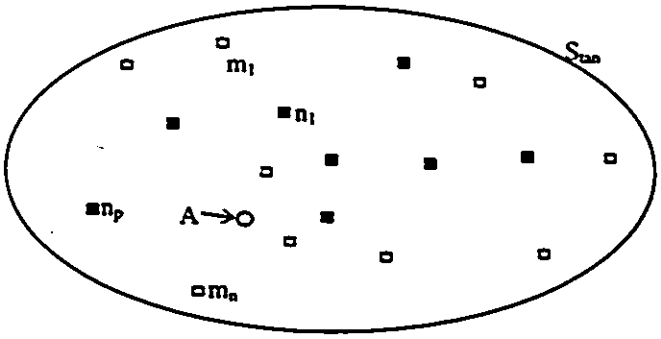

Figure 5 Joint solution domain

This situation is depicted in Figure 5, where only the point A remains unchanged along with other overlapping minima points from S_θ and S_ϕ . This is obvious since the Euclidean norm preserves the relative distances between possible distributions and the solution domain is defined for positive values only.

The square root norm acts as a filter, removing all minima that do not belong to both S_θ and S_ϕ . In another words, if for a particular distribution there is a local minima present in both domains, a local minima will also be present in the joint domain. It is be noted that the inverse is not true: if the joint domain presents a local minimum, the original domains will not in general also present a minimum for the same choice of phase distribution. Also, even though there are less secondary minima or traps for the joint domain, the same observations as to the case depicted by Figure 3 apply.

A very natural question that arises is whether we absolutely have to join the S_θ and S_ϕ distributions. The first observation is that the sets $\{S_\theta\}$ and $\{S_\phi\}$ are not independent of each other since they were both derived from the same unknowns (see 3.4.2). The second observation is that once a solution has been found for either of S_θ or

S_ϕ, it also has to be a solution to the other distribution, otherwise we can safely reject it as a secondary minimum. Building a *cascading* algorithm, where after some iterations, the next approximation of the coefficient distribution is fed into a process that works exclusively with one solution domain, will hopefully be more robust than a standard functional that minimizes over only one domain, namely S_{tan}. The obvious limitation are the cases for which local minima overlap, in which case the algorithm gets trapped, just as it would behave over S_{tan} domain. In that instance unfortunately, there is no apparent solution. Another foreseeable trapping problem can possibly happen even without presence of local minima on S_θ and S_ϕ, as shown in Figure 6.

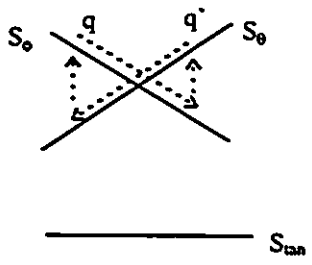

Figure 6 Oscillation trap

In this particular case, with a starting point q, the search algorithm would descend upon the S_ϕ domain, then initiate a search on S_θ with a starting point q' bringing it back to the q point. We notice however that the joint domain does not have to present any local minima, as would be for a simple addition of disjoint domains. This can be avoided be implementing an algorithm with unequal numbers of iterations over each domain, possibly generated randomly.

The above discussion is easily ported to the case of radiated electromagnetic fields. The coefficient retrieval algorithm is presented in Figure 7.

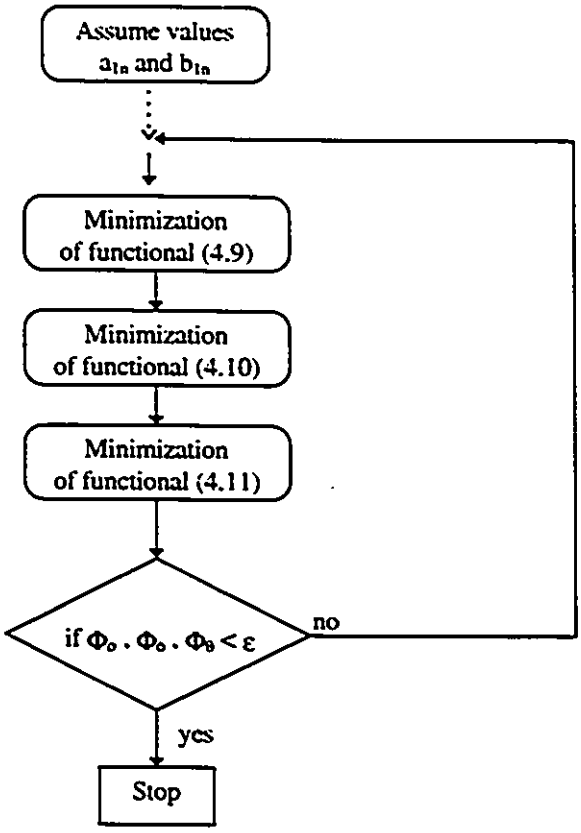

Figure 7 Coefficient retrieval algorithm

Note that we have to rearrange the equation (4.8) into disjoint functionals. The ρ-domain is included, and although not necessary from the uniqueness theorem, it will bring another dimension to the search algorithm.

The minimization process uses the method described in section 4.5. Because we have no guarantee of finding the absolute minimum, the process has to be initiated with different 'guesses' at the (a,b) coefficients, rendering the proposed method heuristic.

$$\Phi_\rho(a_{1n},b_{1n}) = norm\left(\left\|E_{B\rho}\right\| - \begin{bmatrix} M_{1n}^{\rho} & N_{1n}^{\rho} \\ M_{1n}^{\rho+1} & N_{1n}^{\rho+1} \end{bmatrix} \begin{bmatrix} a_{1n} \\ b_{1n} \end{bmatrix}\right) \tag{4.9}$$

for radial propagation,

$$\Phi_\theta(a_{1n}, b_{1n}) = norm\left(\|E_{B\theta}\| - \begin{Vmatrix} M_{1n}^{\theta} & N_{1n}^{\theta} \\ M_{1n}^{\theta-1} & N_{1n}^{\theta-1} \end{Vmatrix} \begin{Vmatrix} a_{1n} \\ b_{1n} \end{Vmatrix} \right) \tag{4.10}$$

for axial propagation and,

$$\Phi_\phi(a_{1n}, b_{1n}) = norm\left(\|E_{B\phi}\| - \begin{Vmatrix} M_{1n}^{\phi} & N_{1n}^{\phi} \\ M_{1n}^{\phi-1} & N_{1n}^{\phi-1} \end{Vmatrix} \begin{Vmatrix} a_{1n} \\ b_{1n} \end{Vmatrix} \right) \tag{4.11}$$

for azimuthal propagation, all with obvious notational changes.

The rows of the wave expansion matrix now represent one of the three coordinate measurements on the second surface. As mentioned previously, the initial guess is generated randomly for the lack of any valid *a priori* knowledge of the expansion coefficients.

The iterations are performed sequentially on the ϕ, θ and ρ amplitude components with an initial guess of the expansion coefficients. As the constrained optimization searches for the solution the new coefficient approximations are fed back to the algorithm. As mentioned previously, we are trying to converge to a solution from different directions. There is no mathematically defined number of optimum iterations over a particular domain, but we are trying to insure that each iteration finds some minima. This minima will then be validated by searching over the other domains.

We notice however, that with this approach only the amplitude measurements on the second surface are used whereas we have such measurements from the first surface available as well. We can use this information through equations (4.3) and (4.4) to obtain bounds for the (a,b) coefficients respectively. Those bounds will limit the solution domain by imposing constraints on possible values (a,b) can assume. The development for the a_{1n} coefficient proceeds as follows: since for a complex number,

$$\|z_1 + z_2\| \le \|z_1\| + \|z_2\| \tag{4.12}$$

by induction,

$$\|z_1 + z_2 ... + ... z_n\| \le \|z_1\| + \|z_2\| ... + ... \|z_n\| \tag{4.13}$$

so we obtain from (4.3).

$$a_{1n} \le \frac{2\pi}{I}\frac{\pi}{J}k_{1n}\sum_{i=0}^{I}\sum_{j=0}^{J}\left\|M_{1n}(i,j)\right\|\left\|E_{A\tan}(i,j)\right\|\sin(\tfrac{i\pi}{I}) \qquad (4.14)$$

and bounds for the b_{1n} coefficient are obtained in the same manner. Equation (4.14) gives a finite bound for a_{1n} since all involved functions are finite in the region of interest. Obviously, the same bounds apply to either of the equation (4.9), (4.10) or (4.11).

The final formulation is stated accordingly: minimize either of equations (4.9) through (4.11) such that (4.14) holds. We notice that the phase distribution is not found at all. Instead we estimate the coefficients that are function of this distribution. The problem to solve is clearly reduced: from a case where the number of unknowns is large and not well defined (we need the samples for numerical integration), we pass to one where they are well quantified and related to the physical size of the radiating device. Furthermore, simplification [19] can be obtained from the orthogonality property of the sinusoid functions (applied to equations (3.44) and (3.45)).

4.4 Spherical Coordinates Implementation

Although easy formulation is achieved when expressing the equations mathematically, they still need to be implemented on a computer for simulations and validation results.

The Coordinate system

Some encountered problems were as trivial as transforming values from Cartesian to spherical coordinates. This stems from the fact that each point can be uniquely represented in spherical coordinates, except for the points where the axial angle is equal to zero. This problem occurred for the construction of the validation field where calculations were made for sources not on the coordinate origin. Another modification required the transformation from spherical to Cartesian coordinates in order to compute the inner product between two vectors.

The coordinate system is defined as in Figure 8 and the notation is applicable in the subsequent sections.

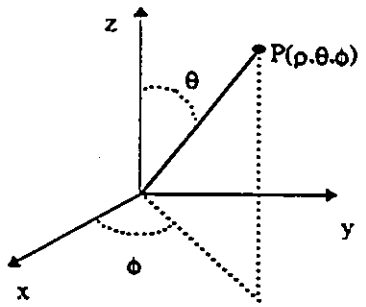

Figure 8 Coordinate system

Spherical Hankel Functions

For the present need, only the Hankel function of the second kind need to be used since we are interested in *outward* traveling waves. The following relationship between the Bessel and Hankel functions exists in cylindrical coordinates,

$$h_n^{(2)}(x) = J_n(x) - iY_n(x) \tag{4.15}$$

where $h_n^{(2)}$ is the cylindrical Hankel function of the second kind.

An additional transformation has to be applied to the equation (4.15) in order to obtain the spherical Hankel function [19],

$$h_n^{(2)}(x) = \sqrt{\frac{\pi}{2x}}\left[J_{n+\frac{1}{2}}(x) - iY_{n+\frac{1}{2}}(x)\right] \tag{4.16}$$

Numerical integration

The integral in equations (3.44) and (3.55) will be approximated by a summation in equations (4.3) and (4.4). Various numerical integration techniques exist such as the trapezoidal rule, Simpson's and Gaussian quadrature. The method applied, however is the

simplest one, the rectangular rule. Since the assumption was that the field over the first surface is readily available, the error introduced is minimal but the computational complexity is reduced. If not enough measurements are available, field interpolation techniques discussed in Chapter 2 can be used to obtain a sufficient number of amplitude data points.

4.5 Optimization techniques

The minimization of equations (4.9) through (4.11), depends on many variables and represent a measure of 'closeness' of the complex problem statement. We have to choose the optimization method based on the usual constraints: accuracy and rapid convergence. The optimization methods guarantee to find values for variables that will minimize some 'cost' function. As such, those methods are *algorithmic*. Because the function to minimize will usually be convex, the obtained minimum can be a local or a global one: only *a posteriori* analysis will tell which was attained. Different variable values will be produced depending on factors more relying on chance rather than mathematics: the process therefore becomes *heuristic* as there is no proof that a particular solution is the desired or best solution.

There are two basic strategies to envisage when faced with minimization problem. The first is the 'divide and conquer' principle, whereby the problem is subdivided into smaller problems of manageable size, each of which is solved independent of each other. The complete solution is obtained by putting the individual solutions together. Obviously, for the method to be valid, the subproblems must be naturally disjoint. The second resides in the iterative improvement. We start in a known system state, and a standard rearrangement is applied to all parts of the system until a new and better state is found. The new state becomes the new configuration and the process continues until no further improvement is possible. The process is usually carried several times, each with a different starting configuration and the best result saved.

First we note that we can set up the problem as a *constrained* optimization, in which case we would use Sequential Quadratic Methods (SQP), or as an unconstrained problem, where a simple functional minimization will suffice. This is the method proposed for the presented algorithm since the bounds on the (a,b) coefficients are easily implemented as constraints.

The goal in SQP optimization is to transform the problem at hand into an easier sub-problem which can then be solved and used as the basis of an iterative process. Methods focusing on the solution of the Kuhn-Tucker equations, which provide the necessary conditions for optimality, are the basis for nonlinear programming algorithms. Those methods are known as the SQP, where a quadratic programming sub-problem is solved at each major iteration, and are very efficient, accurate and produce successful solution over a large set of optimization problems.

An efficient implementation [36] is composed of the following:

- update of the Hessian matrix of the Lagrangian functions using a quasi Newton updating method,
- quadratic programming problem solution,
- line search and merit function calculation.

For a detailed treatise on the above points, the reader is referred to [37] [38].

We can also view the problem as a simple minimization procedure, or finding the roots of a system of non-linear equations. In this instance, either the Gauss-Newton or Lavenberg-Marquardt methods can be applied. The third possibility, the mixed cubic/quadratic polynomial method is dependent on the availability of analytic derivatives from a computational efficiency point of view. The first two methods utilize a search direction function which is obtained from linear least squares problem (Gauss-Newton) or from the solution of linear set of equations (Lavenberg-Marquardt).

Both methods present good characteristics but do not guarantee the uniqueness of attained solution. For a more detailed discussion, [39] presents the details of the above

mentioned methods. Another algorithm implementation is the simulated annealing procedure described in [49]. Note that this method can be quite robust, but the trade-off is the important computing time requirement.

4.6 Validation Field

For validation the simulation will be performed in the following manner: an array of ideal dipoles will be used to generate data in the near-field for values of $0 \leq \theta \leq \pi$, $0 \leq \phi < 2\pi$ and variable ρ. In a practical application where a device under test resides on a (perfect) ground plane, the image theory can be used to find the value of the radiated field below the ground plane. The far-field radiation produced by the same array will be used to validate the simulation, that is, the coefficient retrieval and the subsequent near to far-field transformation.

Field generated by an ideal dipole

The term ideal dipole refers to an infinitesimally short (or of small finite length such as $\Delta l << \lambda$) piece of uniform amplitude current. It does not exist by itself, but may be viewed as a piece of current on an actual radiator [16]. The magnetic field produced by ideal dipoles coincident with the Cartesian system of coordinates is shown in a mathematical form in Table 3.

Dipole orientation	Magnetic field
along the z axis, centered on the coordinate origin	$\bar{H} = \frac{I\Delta z}{4\pi} j\beta\left(1+\frac{1}{j\beta r}\right)\frac{e^{-j\beta r}}{r}\sin\theta\,\hat{\phi}$
along the y axis, centered on the coordinate origin	$\bar{H} = \frac{I\Delta z}{4\pi} j\beta\left(1+\frac{1}{j\beta r}\right)\frac{e^{-j\beta r}}{r}\left(\cos(\phi)\,\hat{\theta}-\cos(\theta)\sin(\phi)\,\hat{\phi}\right)$
along the x axis, centered on the coordinate origin.	$\bar{H} = -\frac{I\Delta z}{4\pi} j\beta\left(1+\frac{1}{j\beta r}\right)\frac{e^{-j\beta r}}{r}\left(\sin(\phi)\,\hat{\theta}+\cos(\theta)\cos(\phi)\,\hat{\phi}\right)$

Table 3- Magnetic field radiated by an ideal dipole

The produced electric field is obtained from

$$\vec{E} = \frac{1}{j\omega\varepsilon}\nabla \times \vec{H} \tag{4.17}$$

resulting in Table 4,

Dipole orientation	Electric field
along the z axis, centered on the coordinate origin	$\vec{E} = \frac{I\Delta z}{2\pi}\frac{1}{j\omega\varepsilon r}\left(j\beta + \frac{1}{r}\right)\frac{e^{-j\beta r}}{r}\cos\theta\,\hat{r} - \frac{I\Delta z}{4\pi}\frac{1}{j\omega\varepsilon r}\frac{e^{-j\beta r}}{r}\left(\beta^2 - \frac{j\beta}{r} - \frac{1}{r^2}\right)\sin\theta\,\hat{\theta}$
along the y axis, centered on the coordinate origin	$\vec{E} = \frac{I\Delta z}{2\pi}\frac{1}{j\omega\varepsilon r}\left(j\beta + \frac{1}{r}\right)\frac{e^{-j\beta r}}{r}\sin\theta\,\hat{r} + \frac{I\Delta z}{4\pi}\frac{1}{j\omega\varepsilon r}\frac{e^{-j\beta r}}{r}\left(\beta^2 - \frac{j\beta}{r} - \frac{1}{r^2}\right)\cos\theta\sin\phi\,\hat{\theta} + \frac{I\Delta z}{4\pi}\frac{1}{j\omega\varepsilon r}\frac{e^{-j\beta r}}{r}\left(\beta^2 - \frac{j\beta}{r} - \frac{1}{r^2}\right)\cos\phi\,\hat{\phi}$
along the x axis, centered on the coordinate origin	$\vec{E} = \frac{I\Delta z}{2\pi}\frac{1}{j\omega\varepsilon r}\left(j\beta + \frac{1}{r}\right)\frac{e^{-j\beta r}}{r}\cos\phi\sin\theta\,\hat{r} + \frac{I\Delta z}{4\pi}\frac{1}{j\omega\varepsilon r}\frac{e^{-j\beta r}}{r}\left(\beta^2 - \frac{j\beta}{r} - \frac{1}{r^2}\right)\cos\theta\cos\phi\,\hat{\theta} - \frac{I\Delta z}{4\pi}\frac{1}{j\omega\varepsilon r}\frac{e^{-j\beta r}}{r}\left(\beta^2 - \frac{j\beta}{r} - \frac{1}{r^2}\right)\sin\phi\,\hat{\phi}$

Table 4- Electric field radiated by an ideal dipole

The radiation produced by an ideal dipole is easily described mathematically and depending on the parameters r (the distance from the ideal dipole to the observation point) and I (the ideal dipole current excitation) various magnetic field values (both real and imaginary) can be obtained. Adding other ideal dipoles in the same region, the electromagnetic field values will then be computed using the principle of superposition [16].

Methodology

In order to obtain various field configurations quickly, the dipoles were assembled into a configuration shown in Figure 9.

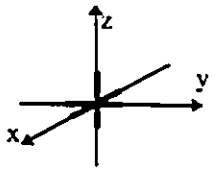

Figure 9 Active dipoles

where each dipole is placed along a coordinate. Each dipole in the array can have a varied complex excitation.

The electric field is generated using an offset from the origin of the coordinate system and source excitation listed in Table 5. By *position*, we mean an offset from the origin in Cartesian coordinates and units are expressed in meters for each coordinate. The *excitation* is multiplied by one thousand (producing larger numbers at the output), one per each dipole as in construction in the Figure 9.

	position	excitation (x 1000)
source #1	0,0,0	1,1,1
source #2	0.2,0.3,0	-j,-j,-j
source #3	-0.2,0.5,0.4	2-j,5-6j,1+5j
source #4	-0.3,-0.1,-0.2	2+2j,10j,-2+3j
source #5	0.3,-0.2,-0.2	-7j,5,4-j

Table 5- Active sources

As will be apparent in Chapter 5, only a few such dipoles suffice to produce very dynamic radiation fields.

Chapter 5

Results

5.1 Introduction

The analysis is performed for the field generated by sources described in Table 5 and for an operating frequency of 1GHz. The near-field is measured at a radius of $r = 1$m, henceforth represented by surface S_A, for values of $0 \le \theta \le \pi$ and $0 \le \phi < 2\pi$ in increments of $\pi/50$ producing a total of (50x100) samples. Note that from the third entry in Table 5 we calculate the radius r_0 of a *minimal* sphere, where $r_0 = \sqrt{0.2^2 + 0.5^2 + 0.4^2} \equiv \frac{2}{3}$ encloses all dipoles. The product of the radius r_0 and propagation constant β is,

$$\lambda = \frac{c}{f} = \frac{1}{3}; \quad \beta r_0 = \frac{2\pi}{\lambda}\frac{2}{3} = 4\pi \tag{5.1}$$

so that at least 13 modes are needed to accurately represent the field through the spherical wave expansion. In the actual implementation, 20 modes are used producing a total of 80 unknowns (see Chapter 3). The radius of the second measurement surface, surface S_B, is $r = 1.1$m. The far-field was calculated on the surface S_C, at a radius $r = 50$.

5.2 Discussion

The generated field yields amplitude distributions as in Figure 10, Figure 12 and Figure 14 for the radial, axial and azimuthal components respectively: this is the information we can obtain by direct measurement of the radiated field and is assumed known. The corresponding phase distributions are presented in Figure 11, Figure 13 and Figure 15 for the same unit vector directions. Of course, this portion of information is not obtained by direct field measurement.

For validation purposes of the spherical wave expansion method, Figure 16, Figure 18 and Figure 20 represent the amplitude of the reconstructed field. Both the amplitude and phase distributions are assumed available on surface S_A. The discrepancy between the fields calculated directly by using formulas in Table 4 ($E_{formula}$) and the reconstructed fields ($E_{reconstructed}$) are shown in Figure 17, Figure 19 and Figure 21 for the respective vector unit coordinates using the norm of the differences,

$$\Delta = \left\| E_{formula} - E_{reconstructed} \right\| \tag{5.2}$$

Very good reconstruction can be obtained as shown by the small absolute error for each coordinate direction. Figure 34 represents the amplitude of the total far-field,

$$E_{far-field} = \sqrt{\left\| E_\rho \right\|^2 + \left\| E_\theta \right\|^2 + \left\| E_\phi \right\|^2} \tag{5.3}$$

obtained through transformation. Equation (5.2) is modified accordingly,

$$\Delta = \sqrt{\left\| E_{f\rho} - E_{r\rho} \right\|^2 + \left\| E_{f\theta} - E_{r\theta} \right\|^2 + \left\| E_{f\phi} - E_{r\phi} \right\|^2} \tag{5.4}$$

and the result shown in Figure 35 Again, results in agreement to the predicted values are produced.

Application of the algorithm presented in section 4.3 yields the results presented for the following cases,

- first case, initial distribution of the coefficients close to the desired solution, obtained by directly calculating the coefficients from equations (4.3) and (4.4) and adding a small random component (±10% of the original),
- second case, initial distribution generated randomly but within the bounds prescribed by equation (4.14).

Results for the radial, axial and azimuthal distributions are presented for the first case in Figure 22, Figure 24 and Figure 26, and for the second case in Figure 28, Figure 30 and Figure 32. Equation (5.2) is applied in all cases and the results are presented for the first

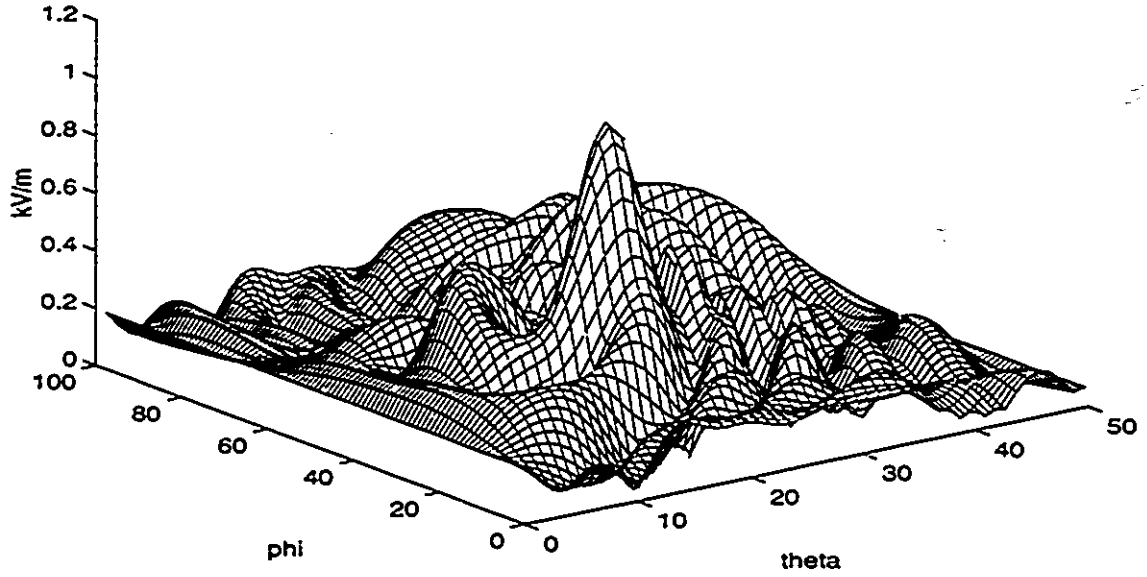

Figure 10 Amplitude of the radial component - validation field

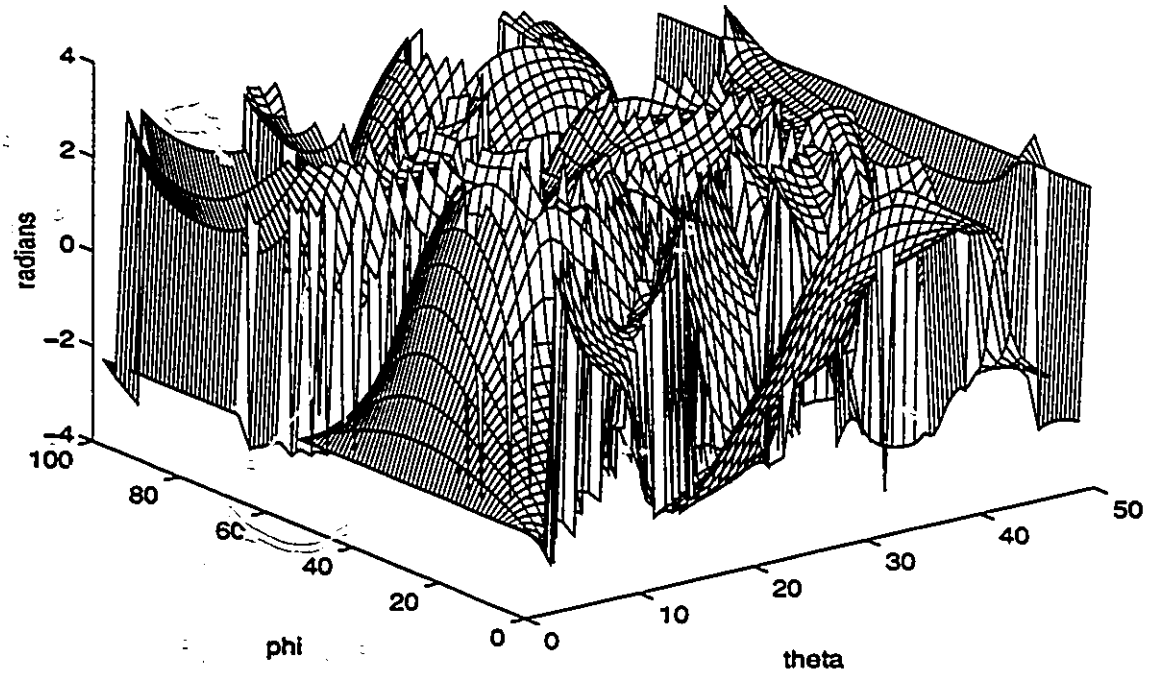

Figure 11 Phase of the radial component - validation field

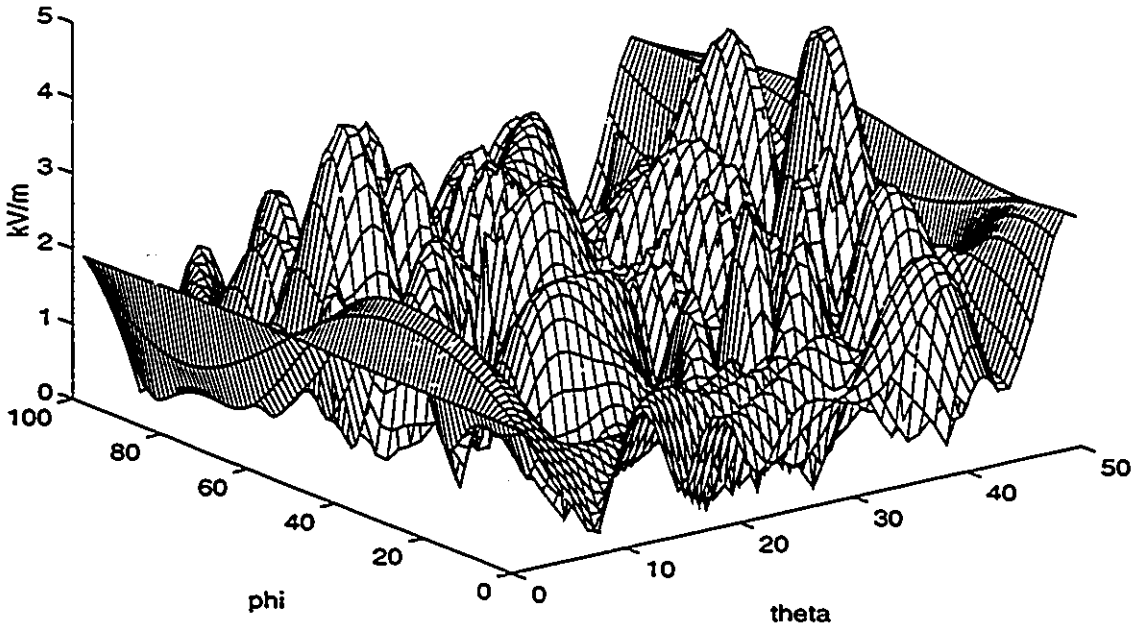

Figure 12 Amplitude of the axial component - validation field

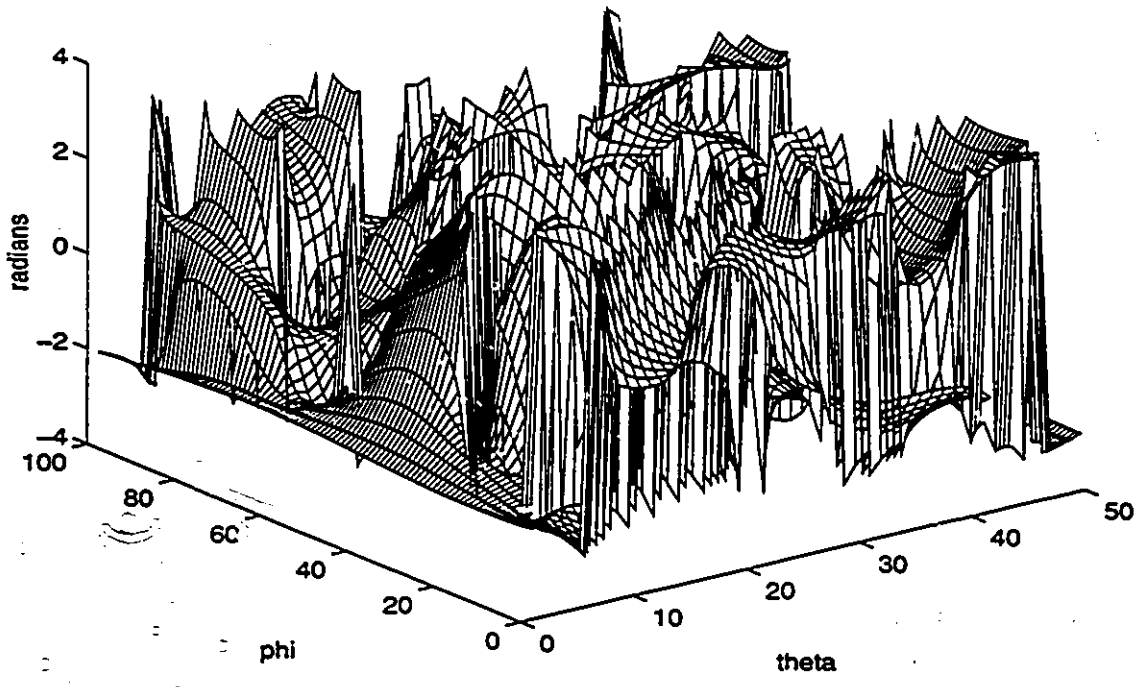

Figure 13 Phase of the axial component - validation field

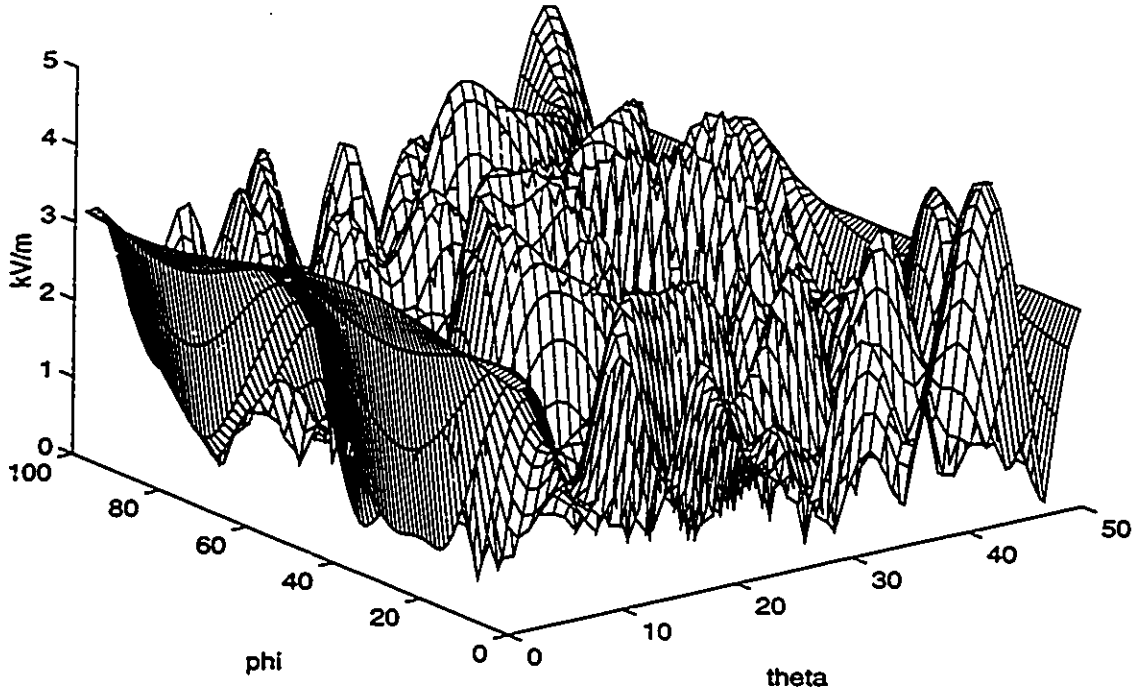

Figure 14 Amplitude of the azimuthal component - validation field

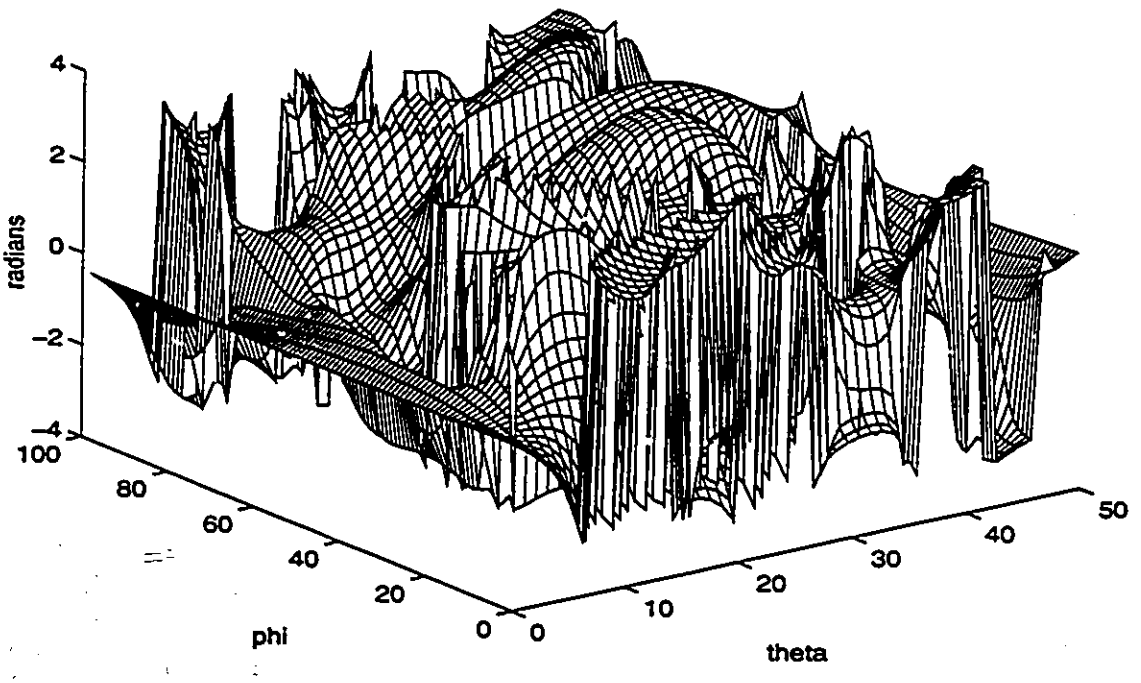

Figure 15 Phase of the azimuthal component - validation field

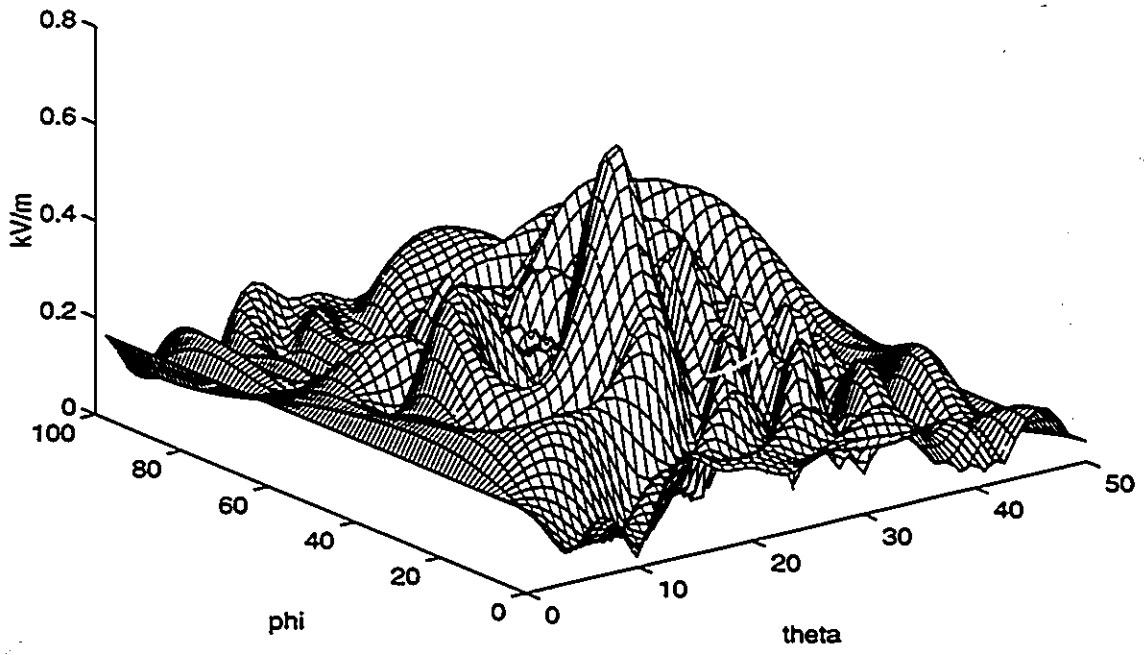

Figure 16 Amplitude of the radial component - reconstructed field

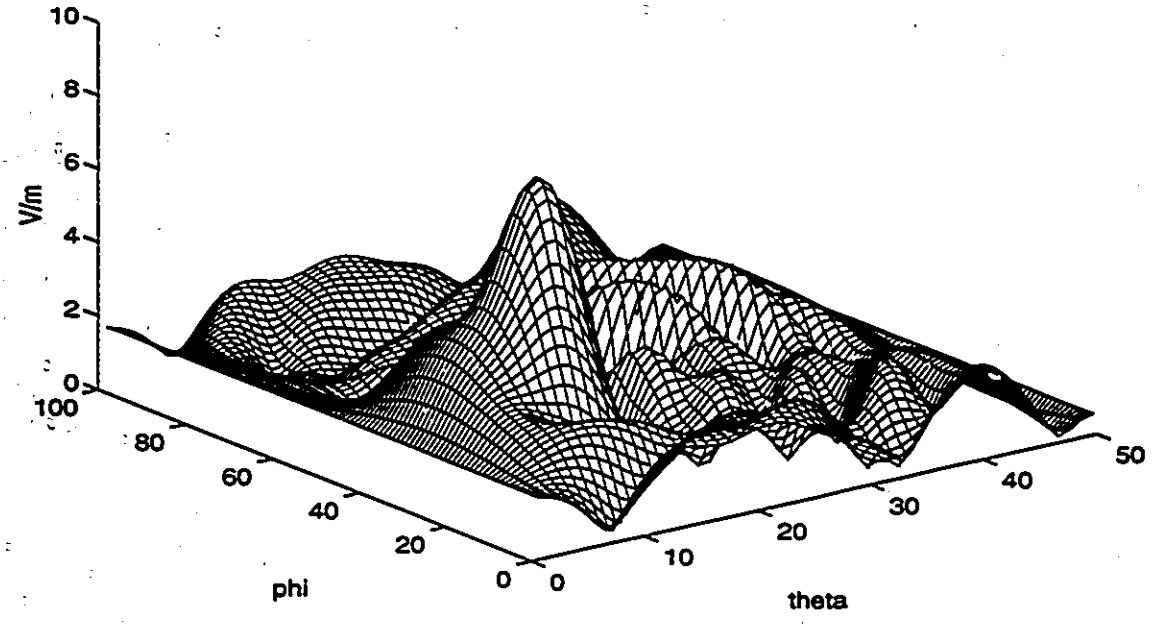

Figure 17 Error of the radial component - reconstructed field

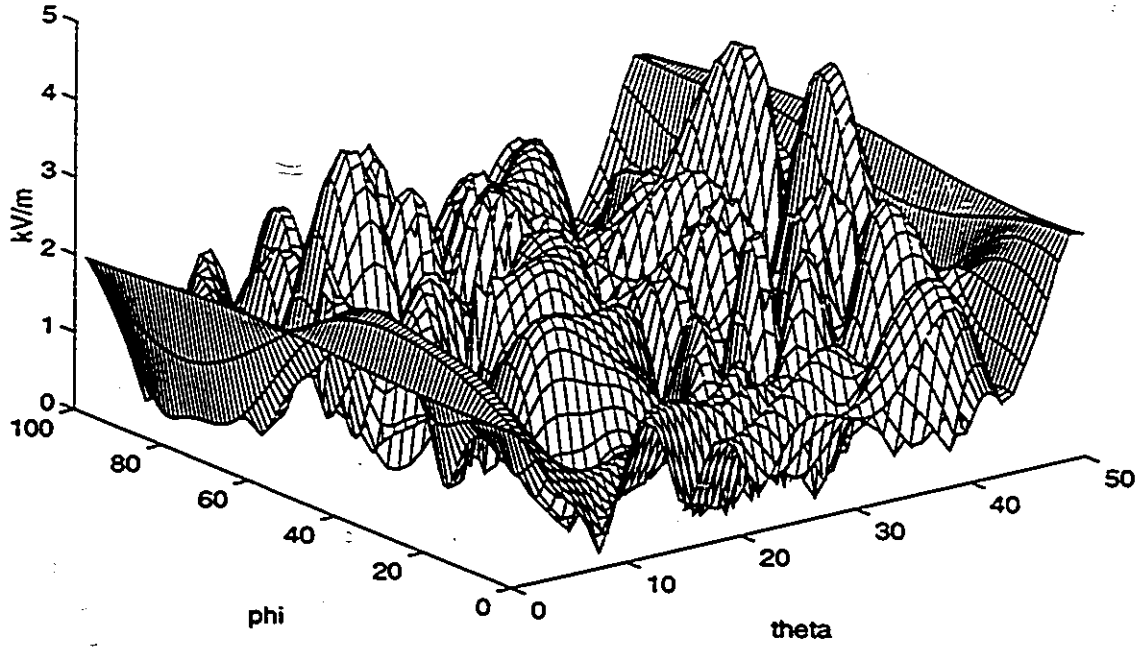

Figure 18 Amplitude of the axial component - reconstructed field

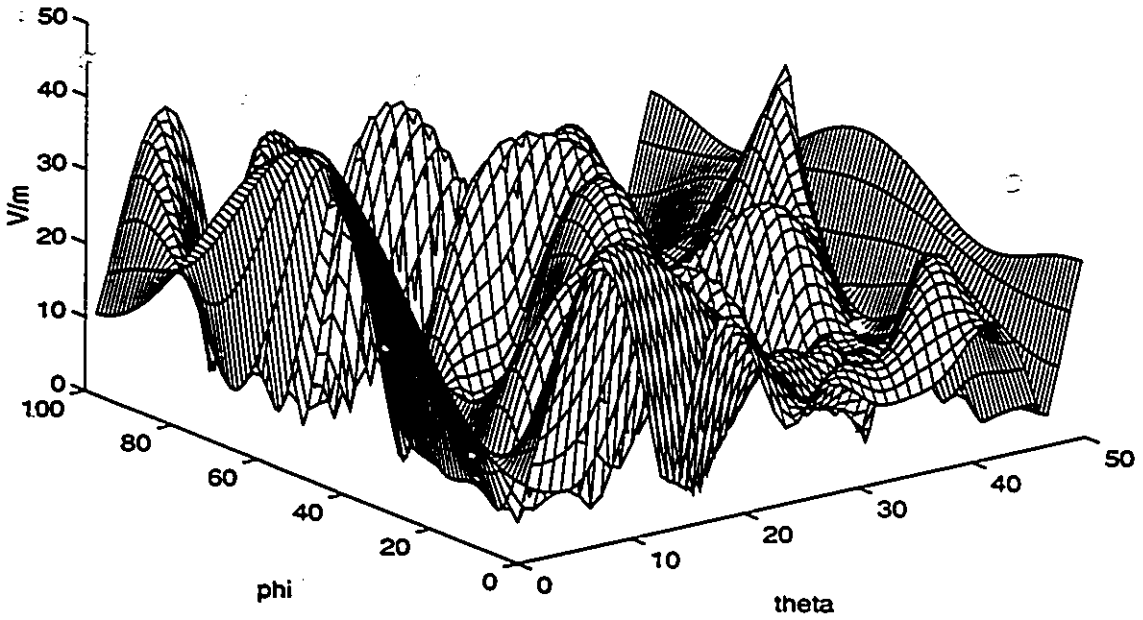

Figure 19 Error of the axial component - reconstructed field

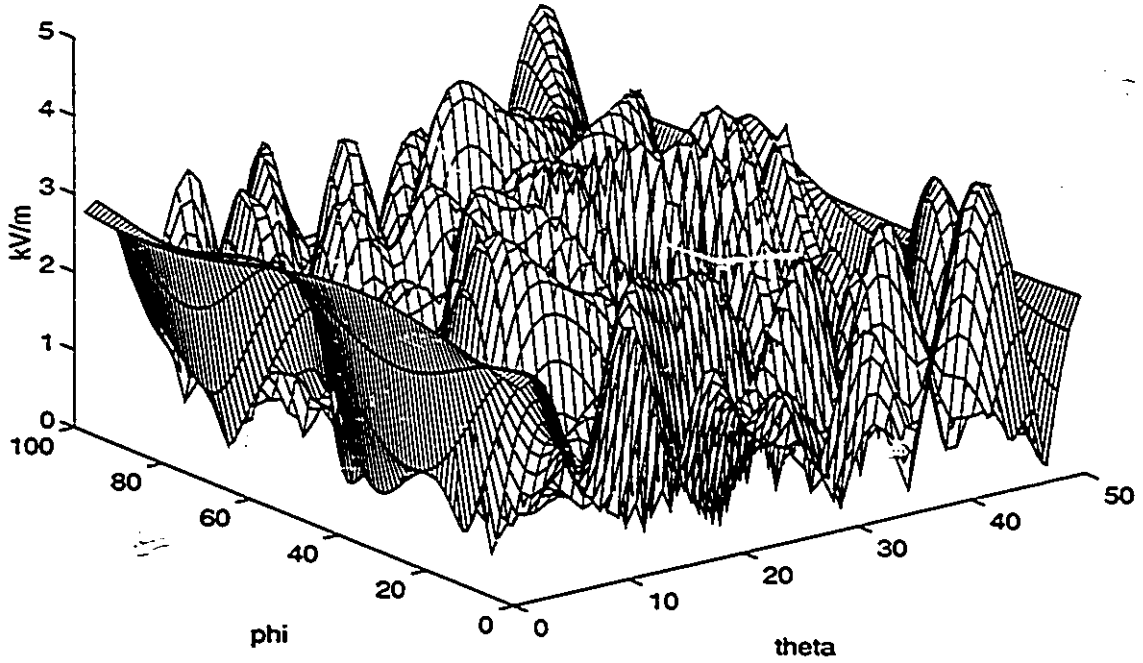

Figure 20 Amplitude of the azimuthal component - reconstructed field

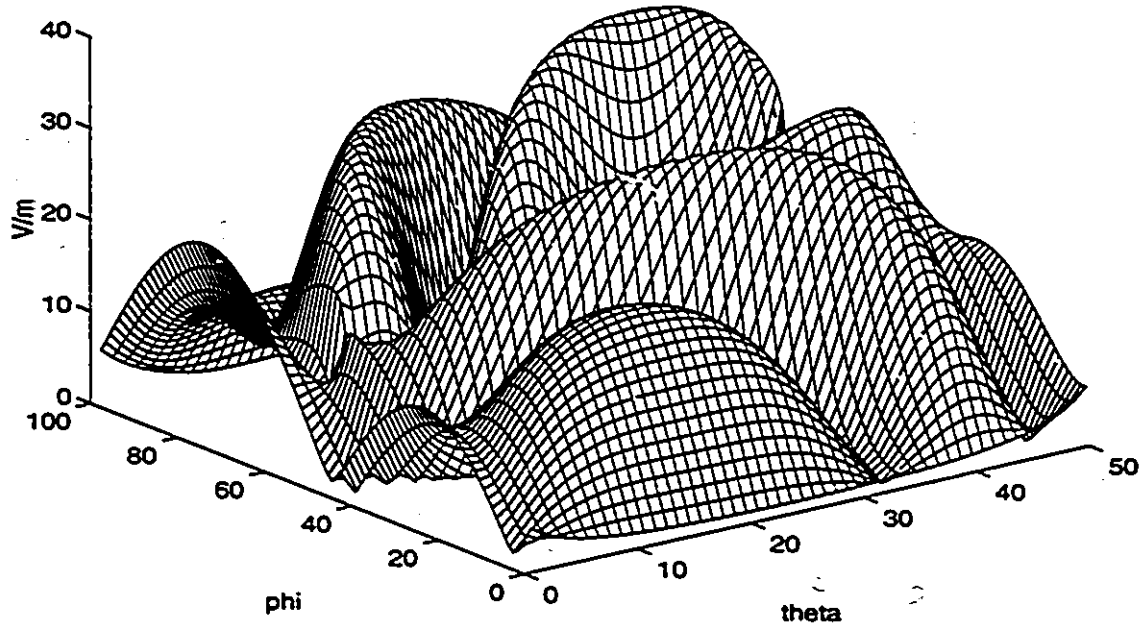

Figure 21 Error of the azimuthal component - reconstructed field

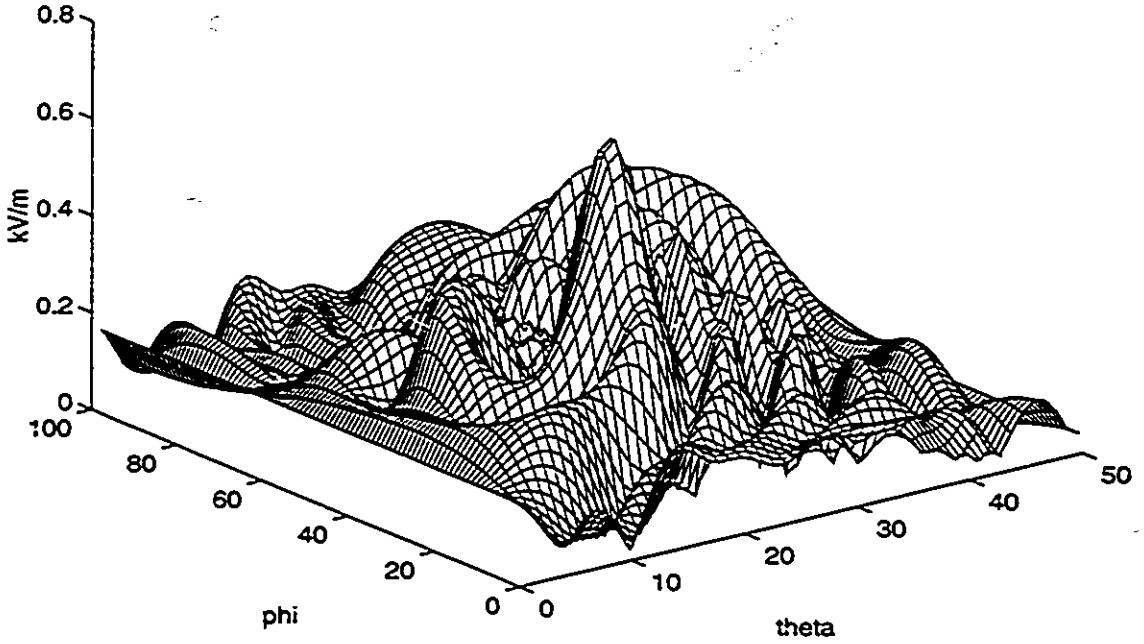

Figure 22 Amplitude of the radial component - first case

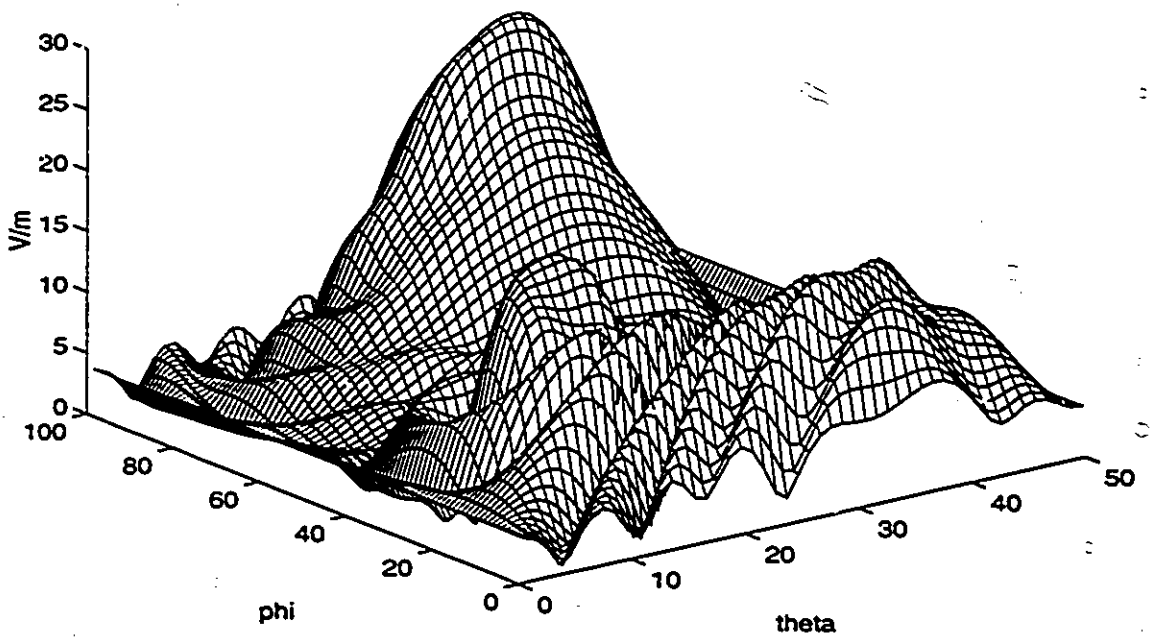

Figure 23 Error of the radial component - first case

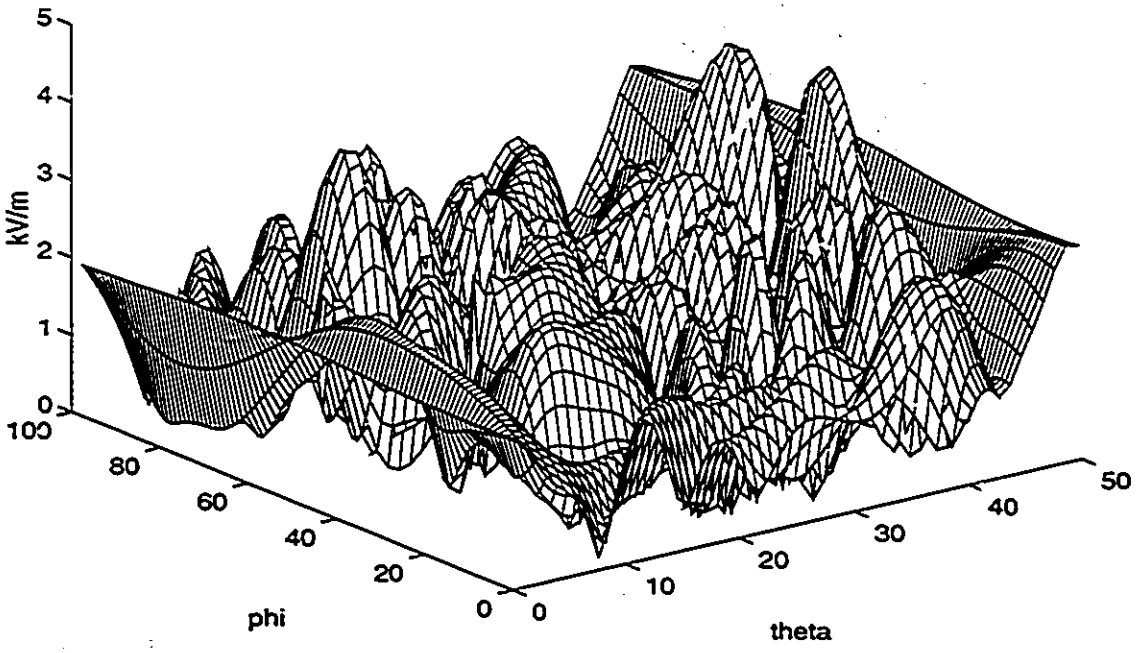

Figure 24 Amplitude of the axial component - first case

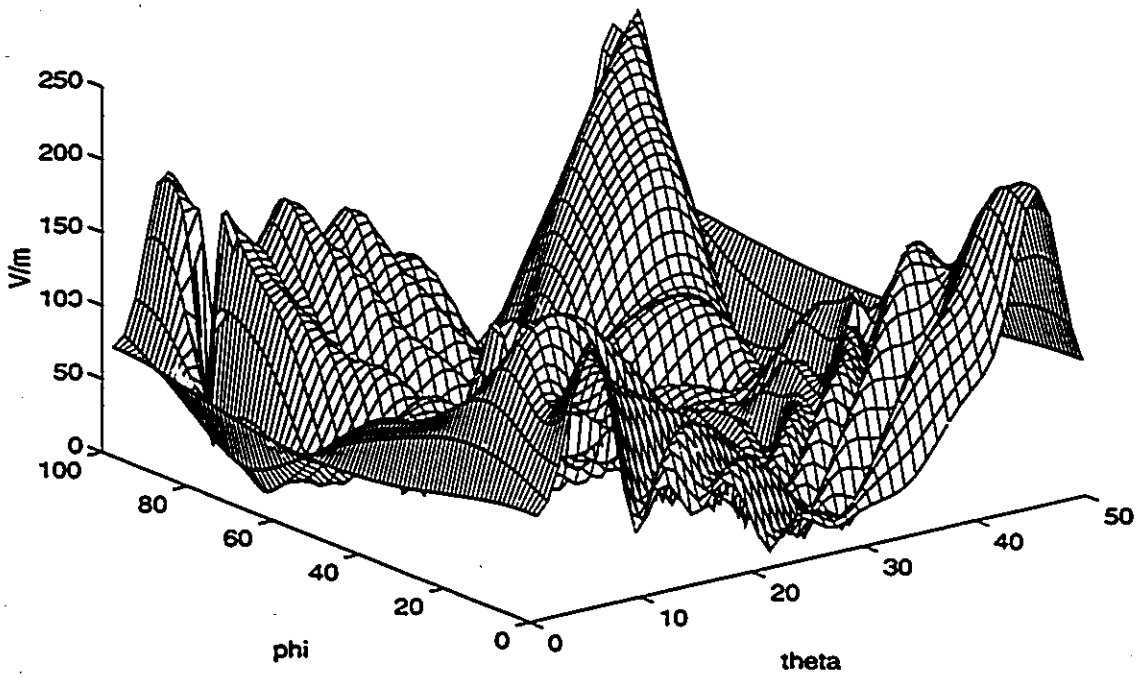

Figure 25 Error of the axial component - first case

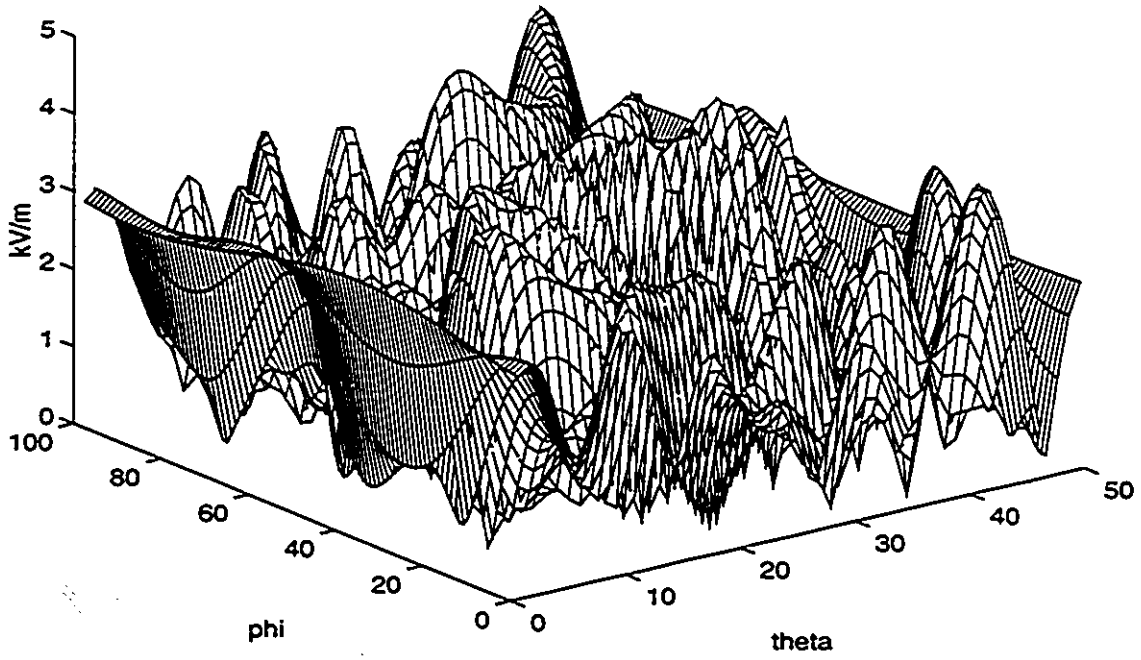

Figure 26 Amplitude of the azimuthal component - first case

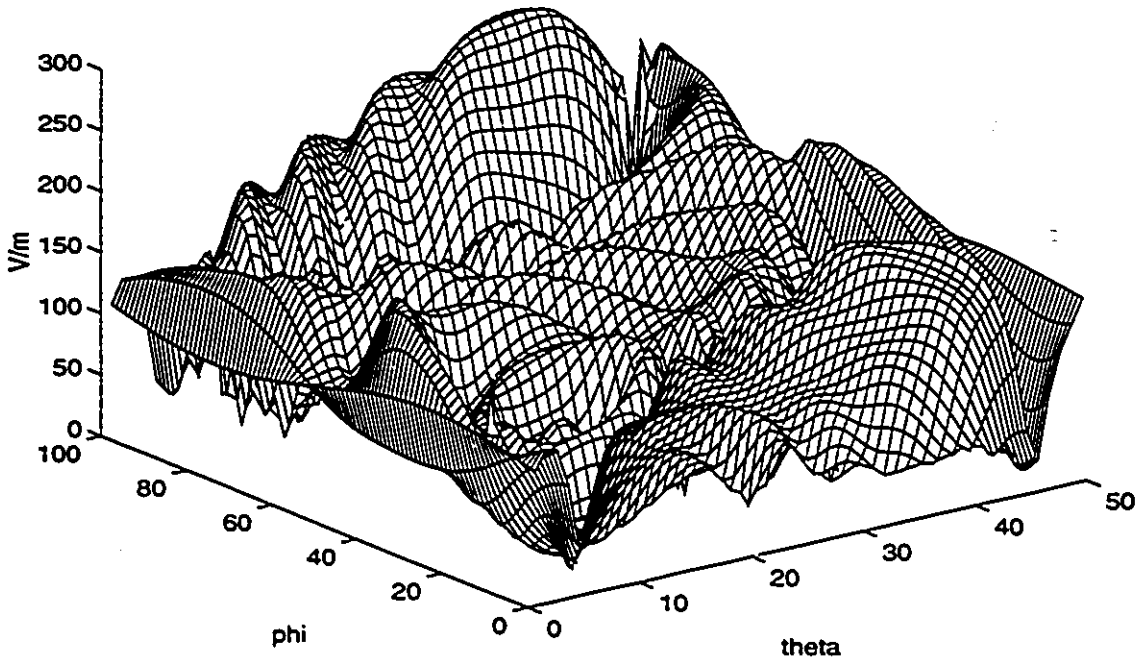

Figure 27 Error of the azimuthal component - first case

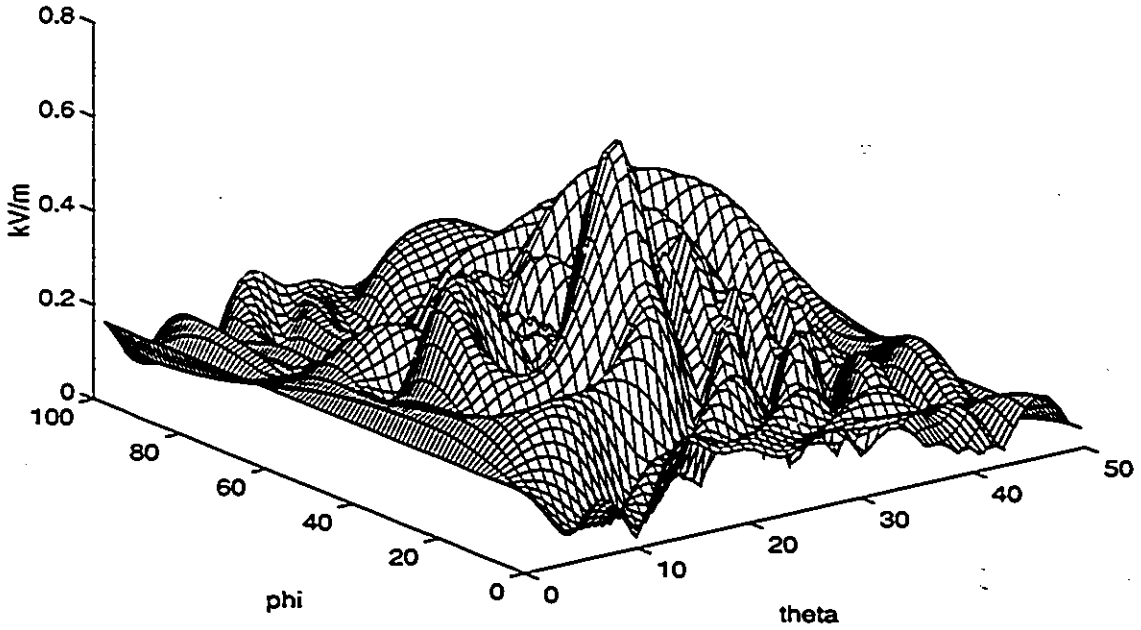

Figure 28 Amplitude of the radial component - second case

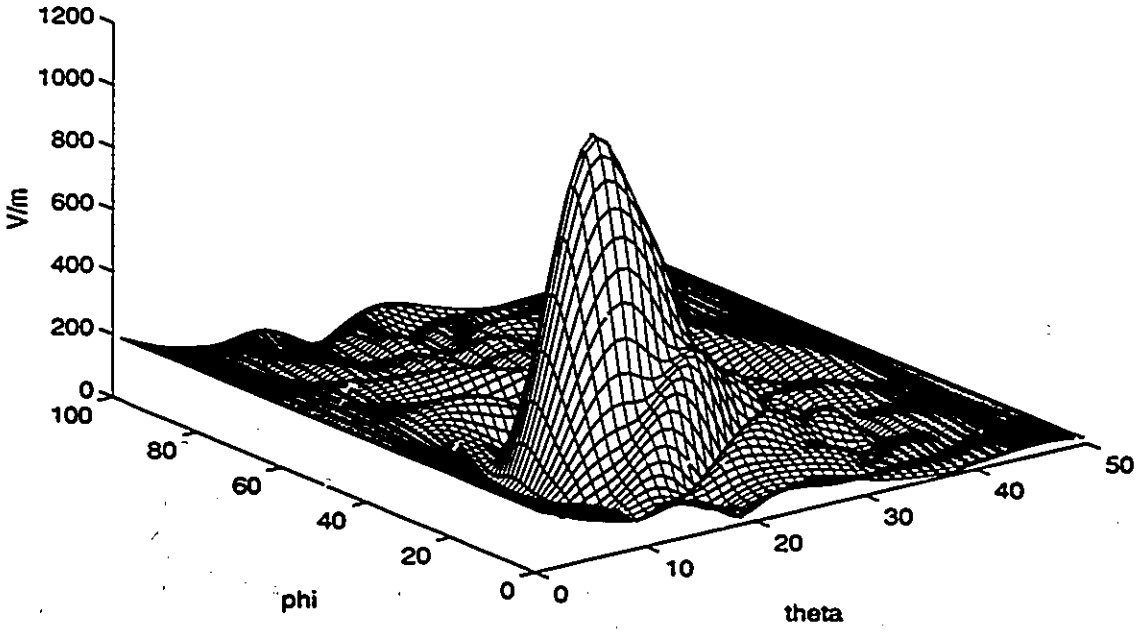

Figure 29 Error of the radial component - second case

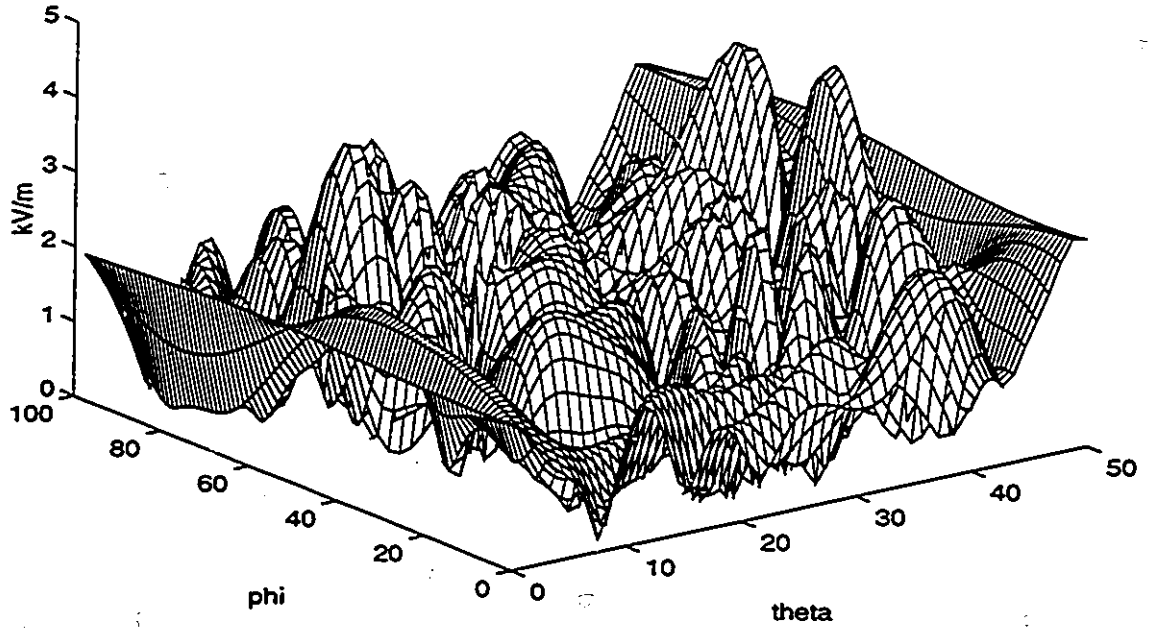

Figure 30 Amplitude of the axial component - ·ond case

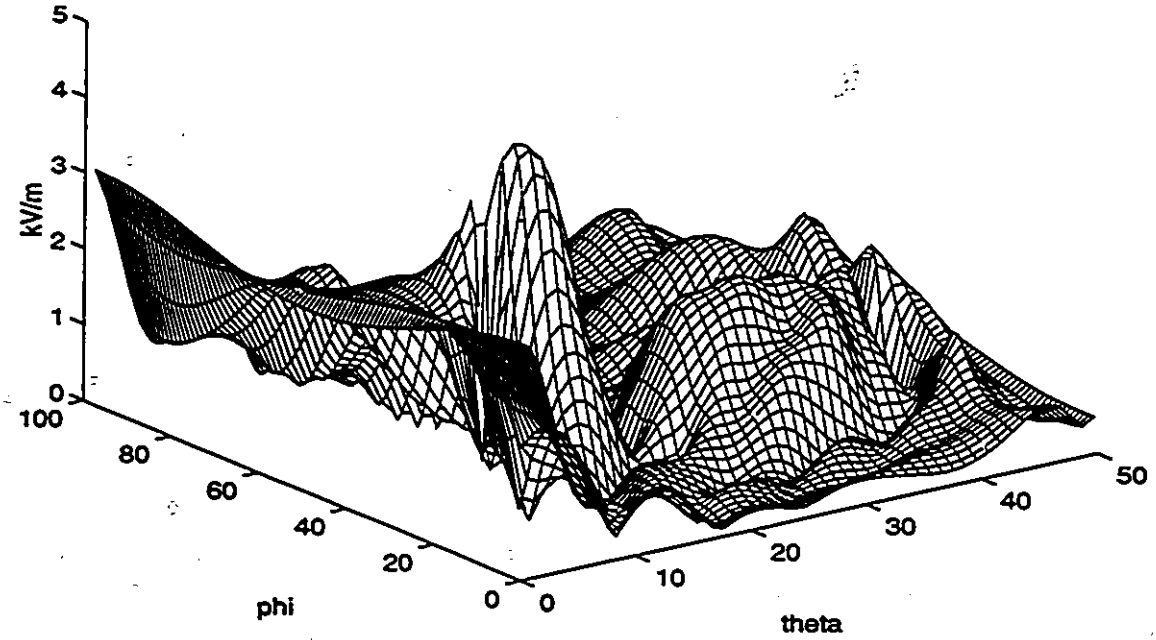

Figure 31 Error of the axial component - second case

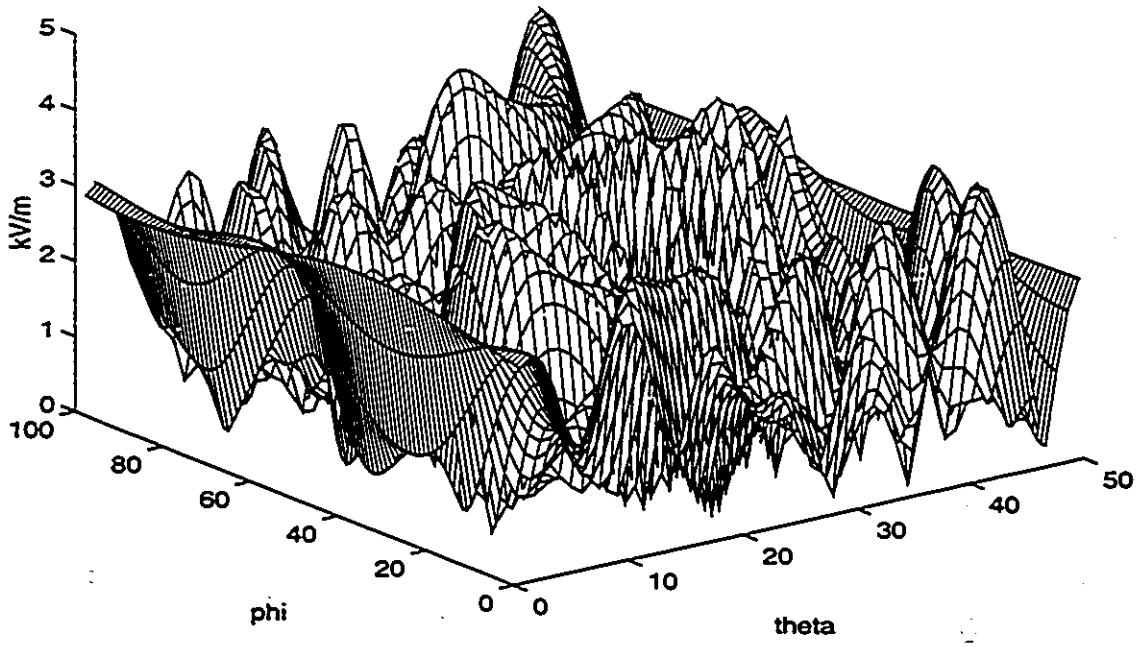

Figure 32 Amplitude of the azimuthal component - second case

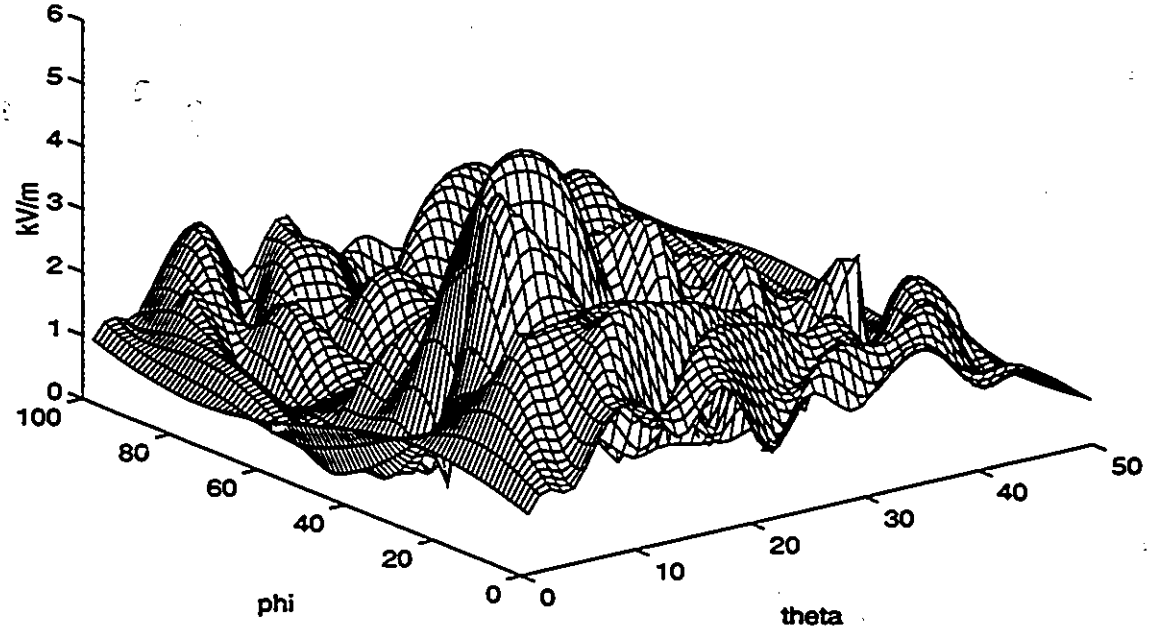

Figure 33 Error of the azimuthal component - second case

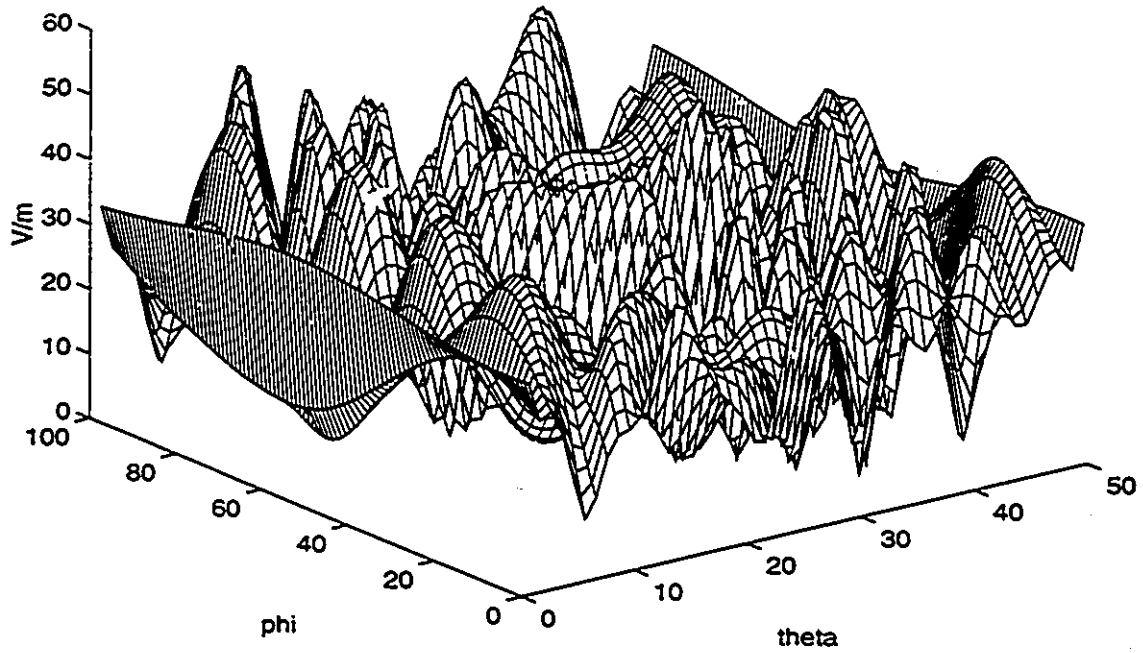

Figure 34 Amplitude of the total far-field - reconstructed field

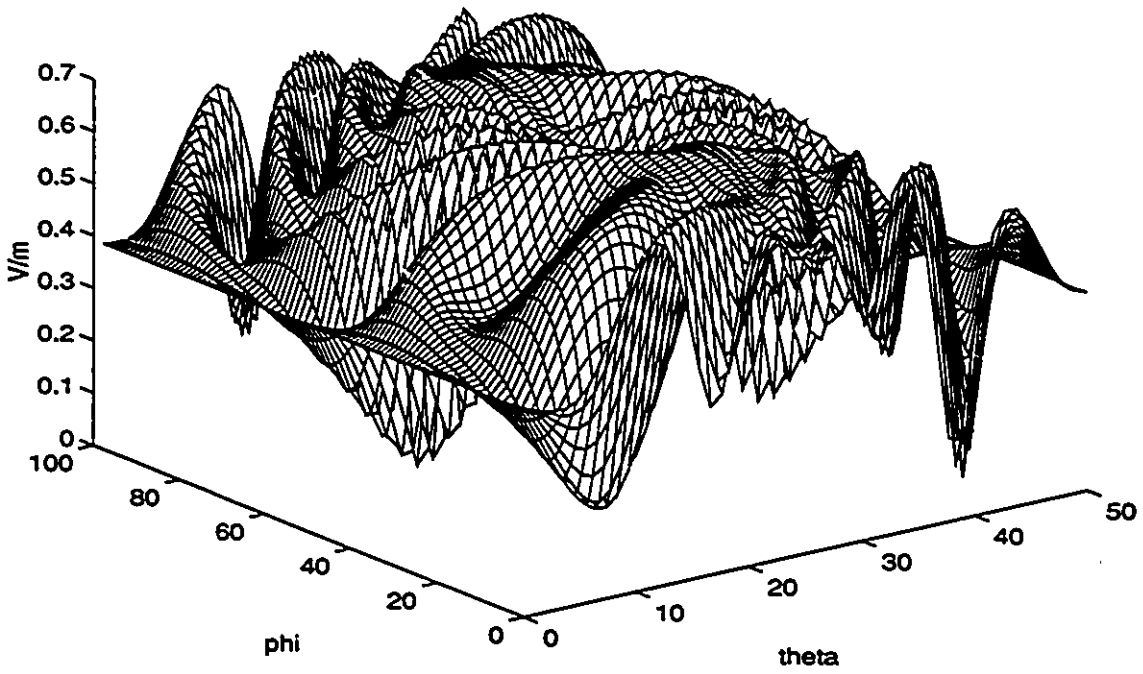

Figure 35 Error of the total far-field - reconstructed field

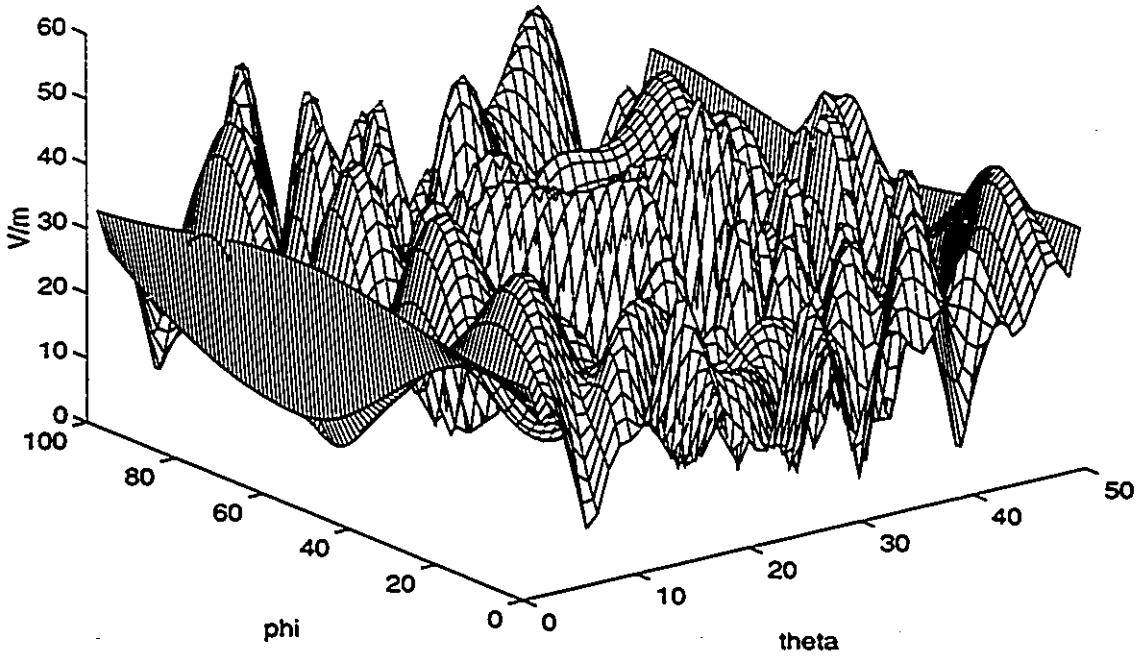

Figure 36 Amplitude of the total far-field - first case

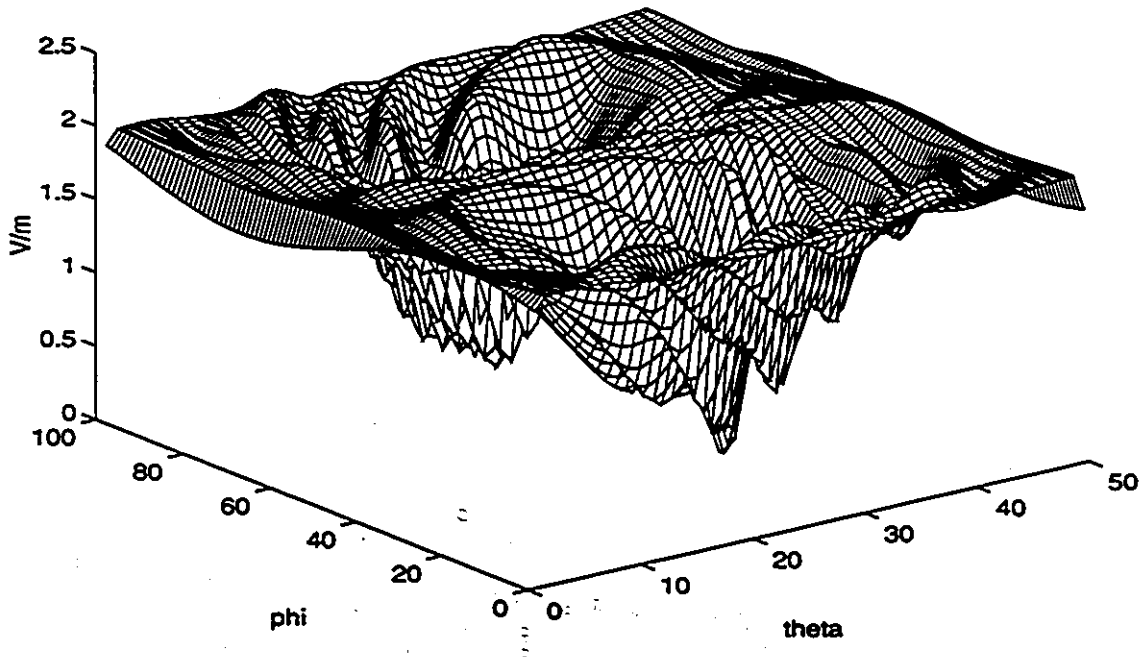

Figure 37 Error of the total far-field - first case

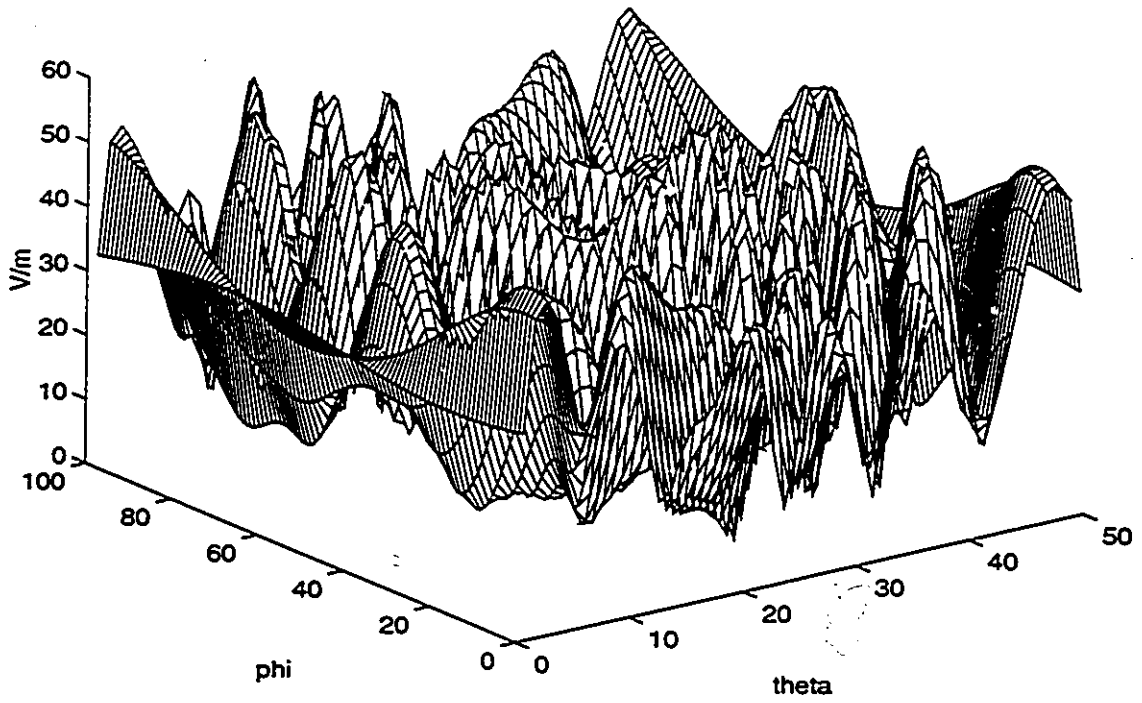

Figure 38 Amplitude of the total far-field - second case

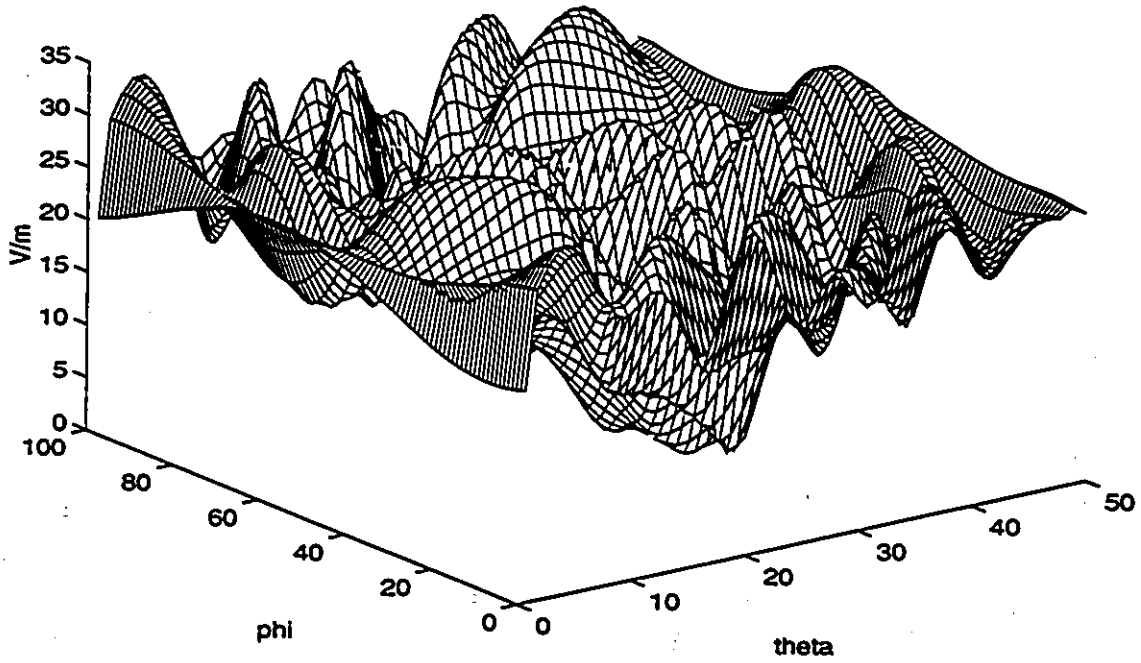

Figure 39 Error of the total far-field - second case

case in Figure 23, Figure 25 and Figure 27, and for the second case in Figure 29, Figure 31 and Figure 33.

Whereas in the first case a proper solution was found, in the second case, the solution was clearly trapped in a local minimum. In another words, a coefficient distribution satisfying equation (4.6) was found, but which does not reproduce the original field with a tolerable amount of error. The situation after transformation to the far-field using the coefficients found in both cases is shown on the next graphs. Again, the total far-field as specified by equation (5.3) is shown. Figure 36 and Figure 37 represent the far field and the error calculated with the expansion coefficients found for the first case, while Figure 38 and Figure 39 represent the second case.

The two described cases are representative of the possible outcomes. It is clear that although we can converge to a solution, it may not be the proper solution. Local minima present therefore a real and serious impediment to the usage of phaseless near- to far-field transformation methods. A proper implementation will reinitiate the procedure with another randomly generated distribution and keep as solution the coefficients best satisfying equation (4.6).

Chapter 6

Conclusion

6.1 Review

The possibility of determining the far-field pattern of radiating systems by measuring their corresponding near-field presents numerous advantages over the direct measurement of the far-field. However, various difficulties inherent to the near-field measurement and its subsequent transformation to the far-field have to be overcome before such methods can be successfully applied to EMI/EMC and antenna characterization problems. The most important necessity is that precise phase measurements of the sampled near-field points be available. A related topic is the size of the resulting problem apparent at implementation. Phase measurements can prove to be difficult, if not impossible to perform. On the other hand, the amplitude measurements can be obtained with a relatively high degree of accuracy at any frequency. The amount of samples necessary to achieve an acceptable level of accuracy will depend on the chosen method of transformation. As a rule of thumb, the more samples we gather, the more accurate results we obtain after the applied transformation. Most of the research in literature deals with simplified cases where the knowledge of the phase distribution is implicitly assumed. Relatively few of the presented methods deal explicitly with amplitude only field measurements, and those that do consider simplified one or two dimensional geometry. The proposed approach considers a general three dimensional case without any assumptions as to the probable radiation pattern, making it suitable for electromagnetic interference and compatibility measurements. The retained approach implements the well known spherical wave expansion technique. The coefficients of the spherical wave functions depend on the boundary conditions, that is the radiated near-field. Due to the incomplete knowledge of this field, only bounds for those coefficients

can be calculated. Application of heuristic methods to the estimation of the coefficients, and upon the assumption of the uniqueness of the solution, is sufficient to fully characterize the radiated fields. Two examples illustrate of the possible outcomes. It is clear that although we can converge to a solution, it may not be the proper solution. Local minima present therefore a real and serious impediment to the usage of phaseless near- to far-field transformation methods. A proper implementation will reinitiate the procedure with another randomly generated distribution of the coefficients and keep as solution the distribution that best minimizes a cost function.

6.2 Future Research

Future research has a few topics to cover. Obviously the algorithm proposed herein can be improved by tightening the bounds on the variables or by supplying an initial set of variables closer to the desired distribution. Another area of research can be a new heuristic method applied to the proposed algorithm, or to another algorithm not necessarily based on the spherical wave expansion.

To expand on the performance of the proposed method, and since it is a heuristic method, experiments have to be performed from which a statistical inference about the performance can be obtained. Comparison with other methods is as yet not possible since to the best knowledge, no existing method takes into account a general three dimensional case.

Bibliography

[1] O. M. Bucci, G. D'Elia, G. Leone, R. Pierri, "Far-field pattern determination from the near-field amplitude on two surfaces", *IEEE Trans. on Antennas and Propagation*, Vol. 38, No. 11, November 1990. pp 1772-1779.

[2] S. Ries, "On the reconstruction of signals by a finite number of samples", *Signal Processing*, Vol. 23, No. 1, April 1991, pp 45-68., Elsevier Science Publishers, B. V.

[3] M-L. Liou, "Spline fit made easy", *IEEE Trans. on Computers*, Vol. C-25, No. 5, May 1976. pp 522-527.

[4] E. Kishon, T. Hastie, H. Wolfson, "3-D curve matching using splines", *Journal of Robotic Systems* 8(6), pp 723-743, John Wiley & Sons, 1991

[5] F. M. Tesche, "On the use of the Hilbert transform for processing measured CW data", *IEEE Trans. on Electromagnetic Compatibility*, Vol. 34, No. 3, August 1992, pp 259-266.

[6] O. M. Bucci, G. Franceschetti, "On the spatial bandwidth of scattered fields", *IEEE Trans. on Antennas and Propagation*, Vol. AP-35, No. 12, December 1987. pp 1445-1455.

[7] ----, "On the degrees of freedom of scattered fields", *IEEE Trans. on Antennas and Propagation*, Vol. 37, No. 7, July 1989. pp 918-926.

[8] D. B. Nguyen, S. Berntsen, "The reconstruction of the relative phases and polarization of the electromagnetic field based on amplitude measurement", *IEEE Trans. on Microwave Theory and Techniques*, Vol. 40, No. 9, September 1992. pp 1805-1811

[9] O. M. Bucci, C. Gennarelli, C. Savarese, "Interpolation of electromagnetic radiated fields over a plane by nonuniform samples", *IEEE Trans. on Antennas and Propagation*, Vol. 41, No. 11, November 1993. pp 1501-1508.

[10] R. Laroussi, G. I. Costache, "Far-field predictions from near-field measurements using an exact integral equation solution", *IEEE Trans. on Electromagnetic Compatibility*, Vol. 36, No. 3, August 1994. pp 189-195.

[11] E. Kreyszig, "Advanced engineering mathematics", Sixth ed. John Wiley & Sons, 1988.

[12] O. M. Bucci, G. Franceshetti, "The role of sampling techniques in antenna measurement", in *Satellite Communication Antenna Technology*, R. Mittra, W. A. Imbriale, E. J. Meanders, Eds. Amsterdam: North-Holland, 1983, pp 561-582.

[13] O. M. Bucci, G. DiMassa, "The truncation error in the application of sampling series to electromagnetic problems", *IEEE Trans. on Antennas and Propagation*, Vol. 36, No. 7, July 1988, pp. 941-949.

[14] O. M. Bucci, C. Gennarelli, C. Savarese, "Optimal interpolation of radiated fields over a sphere", *IEEE Trans. on Antennas and Propagation*, Vol. 39, No. 11, November 1991, pp 1633-1643.

[15] C. A. Balanis, "Advanced engineering electromagnetics", John Wiley & Sons, Inc., 1988.

[16] W. L. Stutzman, G. A. Thiele, "Antenna theory and design", John Wiley & Sons, Inc., 1981.

[17] R. C. Johnson, H. A. Ecker, J. S. Hollis, "Determination of far-field antenna patterns from near-field measurements", *Proceedings of the IEEE*, Vol. 61, No. 12, December 1973, pp 1668-1694.

[18] A. C. Ludwig, "Near-field far-field transformations using spherical wave expansions", *IEEE Trans. on Antennas and Propagation*, Vol. AP-19, No. 2, March 1971, pp 214-220.

[19] P. D. Potter, "Application of spherical wave theory to Cassegrainian-fed paraboloids", *IEEE Trans. on Antennas and Propagation*, Vol. AP-15, No. 6, November 1967, pp 727-736.

[20] W. C. Chew, "Waves and fields in inhomogeneous media", D. G. Dudley, ed., IEEE PRESS series on Electromagnetic Waves, 1995.

[21] T. K Sarkar, S. Ponnapolli, E. Arvas, " An accurate method of computing far-field antenna pattern from near-field measurements", *Antennas and Propagation Symp. Dig.*, Vol 1, Dallas, TX., 1990.

[22] R. C. Baucke, J. D'Angelo, G. Crabtree, "Far-field transforms for finite element frequency-domain solutions", *IEEE Trans. on Antennas and Propagation*, Vol. 41, No. 4, April 1993, pp 511-514.

[23] J. Brown, E. V. Jull, "The prediction of aerial radiation pattern from near-field measurements", *The Institution of Electrical Engineers*, paper No. 3649E, November 1961, pp 635-644.

[24] C. H. Wilcox, "An expansion theorem for electromagnetic fields", *Communications on Pure and Applied Mathematics*, Vol. IX, 1956, pp115-134.

[25] J. A Stratton, Electromagnetic Theory, New York, McGraw - Hill, 1941.

[26] R. J. Luebbers, K. S. Kuntz, M. Schneider, F. Hunsberger, "A finite-difference time-domain near zone to far zone transformation", *IEEE Trans. on Antennas and Propagation*, Vol. 39, No. 4, April 1991.

[27] O. M. Bucci, C. Gennarelli, C. Savarese,"Fast and accurate method of computing far-field antenna pattern from near-field measurements", *IEEE Trans. on Antennas and Propagation*, Vol. 39, No. 1, January 1991.

[28] A. Tennant, G. Junkin, P. Anderson, "Antenna far field predictions from two phaseless cylindrical near-field measurements", *Electronic Letters*, Vol. 28, No. 23, November 5th, 1992, pp 2120-2121

[29] T. Isernia, G. Leone, R. Pierri, "Results for a truncated phaseless near-field technique", *Electronic Letter*, Vol. 39, No. 5, March 4th, 1993, pp 505-506.

[30] W. M. Gordon, "Far-field approximations to the Kirchhoff-Helmholtz representation of scattered fields", *IEEE Trans. on Antennas and Propagation*, July 1975, pp 590-592

[31] M. Khalladi, J. A. Morente, J. A. Porti, G. Gimenez, "Two near- to far-zone approaches for scattering problems using the TLM method", *IEEE Trans. on Antennas and Propagation*, Vol. 41, No. 4, April 1993.

[32] M. S. Narasimhan, K. Varadarangan, "An efficient technique for spherical near-field to far-field transformation and evaluation of far fields of perfectly conducting scatterers", *IEEE Trans. on Antennas and Propagation*, Vol. 37, No. 12, December 1989. pp 1529-1536

[33] J. Romeu, L. Joffre, A. Cardama, "Far-field errors due to random noise in cylindrical near-field measurements", *IEEE Trans. on Antennas and Propagation*, Vol. 40, No. 1, January 1992.

[34] O. M. Bucci, C. Gennarelli, C. Savarese,"Fast and accurate method of computing far-field antenna pattern from near-field measurements", *IEEE Trans. on Antennas and Propagation*, Vol. 39, No. 1, January 1991.

[35] M. Mostafavi, J-C. Bolomey, D. Picard,"Far-field accuracy investigation using modulated technique for fast near-field measurements", *IEEE Trans. on Antennas and Propagation*, Vol. AP-39, No. 3, March 1985. pp 279-285

[36] A Grace, "Optimization Toolbox for use with Matlab", *The Mathworks Inc.*, 1992.

[37] D. P. Bertesekas, "Constrained optimization and Lagrange multiplier methods", *Academic Press Inc.*, 1982.

[38] H. P. Kunzi, G. Tzschach, C. A. Zehnder, "Numerical methods of mathematical optimization", *Academic Press Inc.*, 1971.

[39] "Numerical methods for constrained optimization", P. E Gill, W. Murray, editors, *Academic Press Inc.*, 1974.

[40] W. Martin,"Computation of antenna radiation pattern from near-field measurements", *IEEE Trans. on Antennas and Propagation*, March 1967. pp 316-318

[41] G. D'Elia, G. Leone, R. Pierri, G. Schirinzi,"New method of far-field reconstruction from Fresnel field", *Electronic Letters*, Vol. 20, No. 8, April 1984. pp 342-343

[42] O. Bucci, G. Franceschetti, G. D'Elia,"Fast analysis of large antennas - a new computational philosophy", *IEEE Trans. on Antennas and Propagation*, Vol. AP-28, No. 3, May 1980. pp 306-310

[43] J. Osburn, E. Bronaugh,"Planning for optimal application of broadband, omnidirectional electric field probe system", *The Electro-Mechanics Company*, Austin, Texas, USA.

[44] M. Kanda,"Standard probes for electromagnetic field measurements", *IEEE Trans. on Antennas and Propagation*, Vol. 41, No. 10, October 1993. pp 1349-1364

[45] L. J. Ziomek,"Three necessary conditions for the validity of the Fresnel Phase approximation for the near-field beam pattern of an aperture", *IEEE Journal of Oceanic Engineering*, Vol. 18, No. 1, January 1993. pp 73-75

[46] L. S. Taylor,"The phase retrieval problem", *IEEE Trans. on Antennas and Propagation*, Vol. AP-29, No. 2, March 1981. pp 386-391

[47] M. S. Narasimhan, S. Christopher, K. Varadarangan "Modal behavior of spherical waves from a source of EM radiation with application to spherical scanning", *IEEE Trans. on Antennas and Propagation*, Vol. AP-33, No. 3, March 1985. pp 350-354

[48] H. L. Thal, J. B. Manges ,"Theory and practice for a spherical scan near-field antenna range", *IEEE Trans. on Antennas and Propagation*, Vol. 36, No. 6, June 1988. pp 815-821

[49] S. Kirkpatric, C. D. Gelatt, M. P. Vecchi ,"Optimization by simulated annealing", *Science*, Vol. 220, No. 4598, 13 May 1983.